

1 **Dynamic Environmental Photosynthetic Imaging (DEPI) Reveals Emergent**
2 **Phenotypes Related to the Environmental Responses of Photosynthesis**

5 Jeffrey A. Cruz^{1,2}, Linda Savage¹, Robert Zegarac¹, Christopher C. Hall^{1,3}, Mio Cruz¹,
6 Geoffry A. Davis^{1,4}, Wm. Kent Kovac^{1,3}, Jin Chen^{1,5} and David M. Kramer^{1,2,3}

8 ¹MSU-DOE Plant Research Lab, ²Biochemistry and Molecular Biology, ³Plant Biology,
9 ⁴Cell and Molecular Biology and ⁵ Computer Science and Engineering, Michigan State
10 University, East Lansing, MI

12 **Abstract**

13 Understanding and improving the productivity and robustness of plant photosynthesis
14 requires high-throughput phenotyping under environmental conditions that are relevant to the
15 field. Here we demonstrate a new experimental platform, the dynamic environmental
16 photosynthesis imager (DEPI), for integrated, continuous and high throughput measurements of
17 photosynthetic parameters during plant growth, under reproducible yet dynamic environmental
18 conditions. The use of parallel imagers obviates the need to move plants or sensors, reducing
19 artifacts and allowing simultaneous measurement on large numbers of plants. As a result, DEPI
20 can reveal new phenotypes that are not evident (or cryptic) under standard laboratory conditions,
21 but emerge under progressively more dynamic or fluctuating illumination. We show examples of
22 such “emergent phenotypes” in mutants of *Arabidopsis* that are highly transient and
23 heterogeneous, appearing in different leaves under different conditions and depending in
24 complex ways on both environmental conditions and plant developmental age. These emergent
25 phenotypes appear to be caused by a range of phenomena, suggesting that such previously
26 unseen processes that are critical for plant responses to dynamic environments.

28 Key index words: abiotic stress, chlorophyll fluorescence, biotic stress, imaging, phenometrics,
29 phenomics, photosynthesis

31 Plants live in highly dynamic and unpredictable environments, requiring phenotypic
32 flexibility that is particularly important in photosynthesis for maintaining tradeoffs among the
33 efficiency of light energy capture, resource requirements and availabilities, and the avoidance of
34 deleterious side reactions, especially the production of reactive oxygen species (ROS), when the
35 rate of light capture exceeds photosynthetic capacity. Hence, the photosynthetic machinery is
36 delicately balanced to provide the right amount of energy, at the right times, in the correct forms
37 without damaging or killing the organism¹⁻³. This integrated regulation is particularly important
38 under fluctuating environmental conditions^{3,4} and involves a wide range of regulatory
39 phenomena, including modulation of biophysical properties of light capturing machinery,
40 allosteric regulation of enzymes, post-translational modification of proteins and gene regulation
41 leading to changes in enzyme levels or morphological properties^{3,5,6}.

42 Improving photosynthetic energy capture for increased food and fuel production will
43 require readjustments in this fine balancing, because regulatory processes that prevent
44 photodamage also tend to reduce the efficiency of energy capture, *e.g.* by increasing the
45 dissipation of light energy in the antenna complexes^{7,8}. At the same time, it is imperative that
46 under all conditions productive yield be maximized to offset losses caused by environmental
47 perturbations^{9,10}. Thus, engineering or selecting for useful adjustments in photosynthetic
48 performance will require the understanding of the roles and mechanisms of critical regulatory
49 components of photosynthesis.

50 Plant photosynthesis research has largely been conducted under artificially static
51 conditions, in controlled environment chambers. These “standard laboratory conditions” provide
52 reproducible experimental designs and have greatly advanced our understanding of the
53 biochemical, structural, biophysical, biochemical and physiological bases of the core processes
54 involved in photosynthesis. However, these approaches can miss important components of
55 photosynthesis that are required for robust and efficient photosynthesis in the rich, dynamic
56 environments encountered in the field. In support of this view, recent studies have shown that
57 mutations that disrupt known photosynthetic regulatory processes can have small effects on
58 growth and/or photosynthetic performance under laboratory conditions, but produce strong
59 phenotypes under rapid fluctuations in environmental conditions^{3,5,11}. For example, the *npq4*
60 mutant lacks photoprotective energy dependent exciting quenching (q_E), or the rapid response
61 component of non-photochemical quenching (NPQ), but higher levels of photodamage and

62 corresponding decreases in ‘fitness’ are only seen when grown under fluctuating light or natural
63 environments¹². Similarly, a state transition mutant (*stn7*) and a proton gradient regulation
64 mutant (*pgr5*) do not accumulate photosystem I (PSI) damage until shifted to growth under
65 fluctuating light^{4, 13}. In addition, environmental growth conditions clearly influence the
66 development of photosynthetic capacity over longer time scales^{13, 14}. Collectively, these
67 observations confirm that both long and short-term effects of growth environment must be
68 considered.

69 It is now recognized that detailed phenotyping under appropriate conditions, an approach
70 we term “environmental phenomics,” is critical for understanding and improving plant yield
71¹⁵. Photosynthetic productivity and robustness are determined by highly complex sets of traits,
72 and depend on many interacting factors related to both maximizing efficiency^{7, 8} and coping
73 with environmental stress^{9, 10}. Thus, environmental phenomics requires non-invasive probes of
74 relevant phenotypes that can be applied to many plants over an extensive range of conditions and
75 multiple time frames.

76 There is a vast literature on the application of *in vivo* spectroscopic techniques to plants.
77 Well established methods include gas exchange¹⁶, chlorophyll *a* fluorescence spectroscopy¹⁷,
78 kinetic absorbance and reflectance spectroscopy^{18, 19}, 3D plant imaging^{20, 21}, thermal imaging^{15,}
79²² and hyperspectral radiometry²³. Each of these techniques has provided useful new
80 information, but generally at discrete time points and/or on individual plants or leaves, and there
81 are several major challenges to applying these techniques for phenotype-driven plant screening,
82 selection and engineering for improved photosynthesis. For example, to achieve high throughput,
83 these techniques must be automated but cannot disturb the physiological status of the plants.
84 Some current approaches rely on mechanized transport of plants to sensors or sensors to plants,
85 e.g. the “conveyor” system, typified by the TraitMill™ (GB - CropDesign), the PlantScreen™
86 (Photon Systems Instruments, Inc.) and Scanalyzer™ (Lemnatec, Inc) systems. In the conveyer
87 systems, numerous plants can be grown in special pots on a network of automated conveyor belts
88 that move the plant to enclosed chambers for measurements. This approach has already been
89 used to screen plants for assessing plant architecture, overall biomass, chlorophyll content,
90 drought responses and nitrogen assimilation²⁴. Although valuable, there are several limitations
91 for the conveyor approach, particularly when attempting to assess effects of environmental
92 fluctuations. Funneling the plants into limited number of chambers requires that plants be

measured at different times of the day, obscuring shorter-term variations induced by diurnal cycles or environmental fluctuations. Enclosing plants in measuring chambers can perturb light capture, metabolism and gene expression and mask the effects of applied environmental parameters, by altering light intensity and quality throughout the canopy²⁵, activate touch responses^{26, 27}, induce rapid temperature²⁸ and alter local CO₂ concentrations²⁹. Also, the need to move plants on the conveyor, can severely limit the dimensions of the pots, potentially affecting root growth, nutrient uptake and drought responses³⁰. An alternative approach, developed by several groups, moves cameras and/or sensors above the plants, in chambers or greenhouses³¹⁻³³ or field³⁴, via a system of cranes, vehicles or cables. The mobile sensor approach avoids the requirement for moving the plants and in principle allows more natural soil/root environments. However, the sensors can only monitor a limited number of plants/plots at a time, preventing assessments of rapid, transient or diurnal effects. In addition, these systems require the use of non-growth wavelengths of illumination, potentially perturbing photosynthesis.

The dynamic environmental photosynthesis imager (DEPI) addresses critical limitations in previous technology and enables direct assessment of rapid and long-term responses to dynamic environmental conditions of large numbers of plants in parallel. Although expandable to many parameters, in this work we focus on DEPI measurements of photosynthesis, reflecting photosystem II (PSII) quantum efficiency (ϕ_{II}), light-driven linear electron flow (LEF), dissipative non-photochemical quenching (NPQ) of absorbed light energy, activation of the photoprotective mechanisms through the q_E response, onset of photoinhibition or chloroplast movements by the slow relaxation of NPQ, i.e. the q_I response. Importantly, our approach allows these measurements to be made while maintaining plants under the white (or arbitrary spectral output) LED illumination and environmental conditions that can simulate fluctuations that occur in a natural environment. In this way, DEPI can capture both short- and long-term (developmental) responses to dynamic environmental conditions.

118

119 **Results and Discussion**

120

121 *High sensitivity photosynthetic imaging under dynamic light conditions.*

122 As shown in **Figure 1a** (described in more detail in the Online Methods), the DEPI
123 lighting system uses an array of high intensity white LEDs with optics that collimate the output

124 light thus achieving steady state light intensities in excess of full sunlight ($>2,500 \mu\text{mol photons}$
125 $\text{m}^{-2} \text{s}^{-1}$) at a distance of 1 m from the plants. The lights can also deliver a brief period (0.5 to a
126 few s) of saturating intensity (up to and exceeding $15,000 \mu\text{mol photons m}^{-2} \text{s}^{-1}$) for measuring
127 various chlorophyll fluorescence parameters. Fluorescence excitation light is supplied by an
128 array of monochromatic LEDs. In the current configuration, these probe LEDs are red, but other
129 wavelengths may also be used. Fluorescence images for all plants under the lighting array were
130 captured simultaneously by five charge-coupled device (CCD) cameras outfitted with glass
131 filters that block visible and pass chlorophyll fluorescence in the near infrared.

132 To demonstrate the utility of DEPI to observe previously unseen phenotypes that appear
133 under fluctuating environmental conditions, we measured photosynthetic parameters in a set of
134 wild type and mutant *Arabidopsis* plants over a 5-day period. Over the course of the experiment,
135 we applied ‘ramped environmental perturbation’ (REP) conditions, designed to reveal
136 phenotypes that are not typically apparent under laboratory conditions but appear under more
137 natural fluctuating conditions (**Fig. 1b**). The population of plants was grown under standard
138 growth chamber conditions for 3 weeks and transferred to DEPI. On day 1, plants were exposed
139 to a ‘flat’ illumination day, with constant $100 \mu\text{mol photons m}^{-2} \text{s}^{-1}$ illumination for 16 hours,
140 similar to that used in typical laboratory growth chamber experiments. Next, plants were exposed
141 to ‘sinusoidal’ illumination (day 2), mimicking the kinetics and intensity of solar irradiation
142 changes over a day in the field. In this case, the maximal intensity at simulated noon was $500 \mu\text{mol photons m}^{-2} \text{s}^{-1}$. On day 3, plants were exposed to ‘fluctuating’ light with changes to
143 impose the kinds of light dynamics resulting from occlusion or reflection of sunlight by clouds or
144 leaf movements induced by wind. Specifically, the sinusoidal illumination used on day 2 was
145 punctuated every 30 min with 8-min fluctuation periods of doubled illumination intensity, so that
146 the peak intensity under fluctuating light was $1000 \mu\text{mol photons m}^{-2} \text{s}^{-1}$. On day 4, plants were
147 given one day to recover under flat day illumination (as on day 1), and then on day 5 were
148 exposed again to fluctuating light to test for acclimation responses to the initial fluctuating
149 conditions. Because the illumination treatments were performed in sequence, the effects are
150 likely to reflect both immediate and cumulative effects of individual conditions.

152 Several chlorophyll fluorescence-derived photosynthetic parameters were imaged
153 periodically over the course of the experiment, including the quantum efficiency of PSII
154 photochemistry ϕ_{II} , LEF, NPQ, as well as the rapidly-relaxing (q_{E}) and slowly-relaxing (q_{I})

155 components of NPQ. The q_E component reflects the activation of photoprotective energy-
156 dependent exciton quenching, while the slowly-relaxing component includes contributions from
157 exciting quenching from photoinhibition or the xanthophyll cycle, state transitions and
158 chloroplast movements³⁵⁻³⁸. Under appropriate conditions, it is possible to infer from these
159 measurements the fate of absorbed light, the activation of photoprotection, and the onset of
160 photoinhibition and repair processes, which are critical for understanding the efficiency and
161 environmental responses of photosynthesis³⁹. Kinetically resolved data for representative plants
162 are described below and in **Supplemental Figures 1-5**.

163 The library of plants included wild type Columbia-0 (Col-0) and a series of over 300
164 mutants lines with T-DNA insertions in chloroplast-targeted nuclear genes provided by the
165 Chloroplast 2010 project (<http://www.plastid.msu.edu/>)^{40, 41}.

166 **Figure 2** shows DEPI ‘snapshot’ images of two photosynthetic parameters, ϕ_{II} (**Fig. 2a**)
167 and q_E (**Fig. 2b**) captured simultaneously for 231 individual plants at the onset of rapid
168 fluctuations in actinic intensity that occurred after 18 minutes of illumination on day 3. At this
169 time point, several mutant lines, including SALK_098173, SAIL_115_E08 and SALK_103895
170 showed distinct red and blue false coloring, representing high and low values for photosynthetic
171 parameters. The very high reproducibility of DEPI measurements is evident by comparing the
172 responses of replicates across the chamber. A statistical analysis of integrated values over a full
173 day experiment shows that DEPI can distinguish changes in ϕ_{II} values with standard deviations
174 of 2-3% of average values, e.g. for ϕ_{II} and q_E (**Figs. 2c and 2d**), across individual cameras or the
175 entire DEPI chamber. This high level of reproducibility was maintained over a period of days
176 and was afforded by careful control of environmental and measurement parameters, especially
177 by the use of calibrated, computer control of individual banks of actinic LEDs (see Online
178 Methods).

179 The snapshots in **Figures 2c and 2d** also emphasize that mutation-induced changes in ϕ_{II}
180 and q_E often occur in highly spatially heterogeneous patterns. For example, SAIL_115_E08 and
181 SALK_103895 showed preferential loss of ϕ_{II} and increase in NPQ in the older (outermost)
182 leaves, possibly reflecting the accumulation of photoinhibition or developmental differences in
183 the structural properties or photosynthetic enzyme activities of the leaves³⁹. The appearance of
184 strong heterogeneity shows that it is often not possible to extrapolate photosynthetic performance

185 from data taken at specific locations or averaged over the entire plant, requiring routine
186 application of imaging techniques see also review in³¹.

187 An extensive analysis of the population of the entire library of mutants will be presented in
188 a forthcoming paper. The current work focuses on the use of DEPI for revealing ‘emergent’
189 photosynthetic phenotypes that appear under dynamic environmental conditions, rather than on
190 understanding specific biochemical bases.

191

192 *Effects of changing illumination conditions on photosynthesis averaged over the entire plant.*

193 We first consider simplified DEPI measurements of photosynthetic phenotypes averaged
194 over entire plants. **Figure 2** shows representative data sets from Col-0 and SALK_098173,
195 which harbors a T-DNA insert in AT1G71500 (TAIR, www.arabidopsis.org), coding for a
196 putative Rieske iron-sulfur domain-containing protein targeted to the thylakoid membrane^{42,43}.
197 Recently this protein has been proposed to be a component of photosystem II, and designated as
198 PSB33, responsible for maintaining and stabilizing the PSII light harvesting complex, super
199 complex organization⁴⁴.

200 On continuous or ‘flat’ illumination on day 1, Col-0 showed nearly constant photosynthetic
201 parameters, indicating that the system was able to maintain steady-state photosynthesis over the
202 entire day. Under sinusoidal illumination on day 2, as irradiance increased, ϕ_{II} decreased so that
203 LEF saturated (**Fig. 3a**). Both the half saturation point (about 160 $\mu\text{mol photons m}^{-2} \text{s}^{-1}$) and the
204 maximal LEF (about 84 $\mu\text{mol electrons m}^{-2} \text{s}^{-1}$ at mid-day) were similar to those observed in
205 short-term exposure to saturating light in plants grown under similar conditions⁴⁵, suggesting that
206 the photosynthetic capacity was not diminished by exposure to the sinusoidal light. NPQ and its
207 component parameters q_E and q_I , increased with increasing illumination before mid-day, and
208 recovered as illumination decreased in the evening (**Fig. 3a**), predominantly reflecting the onset
209 of and recovery from photoinhibition^{18,46}. Interestingly, the q_E parameter increased sigmoidally,
210 after a distinct lag period, probably reflecting the non-linear relationship between q_E and the
211 acidification of the thylakoid lumen pH⁴⁵. On the other hand, the q_I component increased almost
212 immediately during sinusoidal illumination, likely reflecting the activation of chloroplast
213 movements, which contribute to the slowly-recovering fluorescence signal NPQ^{35 47}. The F_v/F_m
214 parameter (see dashed lines, **Fig. 3a**), a measure of the maximal quantum efficiency of PSII
215 before illumination in the morning, was measured to be 0.82, consistent with an essentially

216 complete recovery from any photoinhibition that occurred under laboratory chamber
217 illumination.

218 On day 3, Col-0 photosynthetic parameters were strongly dependent on the fluctuating
219 illumination conditions. During the stronger illumination periods, ϕ_{II} was suppressed while NPQ
220 increased, mainly caused by up-regulation of q_E . These effects largely recovered during the
221 weaker illumination later in the day, except for a small residual suppression of ϕ_{II} at the end of
222 the day (**Fig. 3a**), suggesting a partial loss of photosynthetic capacity. On day 4 (flat light), and
223 day 5 (repeat of the fluctuating light day) the photosynthetic parameters for wild type plants were
224 nearly indistinguishable from those on days 1 and 3 (**Fig. 3 and Supplemental Figs. 1 and 2**),
225 with only small changes in F_v/F_M and ϕ_{II} and NPQ. Thus, we can conclude that, despite the fact
226 that the plants were grown under laboratory lighting conditions, the wild type photosynthetic
227 system was largely able to cope with the abrupt perturbations in light intensity on days 2 and 3.

228 On days 1 and 2, the photosynthetic parameters for SALK_098173 were nearly identical
229 to those in Col-0 (**Figs. 3a and b**). Substantial phenotypic differences only appeared on day 3,
230 with the appearance of 1) decreased maximal PSII quantum efficiency (F_v/F_M), indicating a loss
231 of PSII activity; 2) decreased steady-state quantum yield (ϕ_{II}) especially early in the day; 3)
232 decreased q_E responses during high (and fluctuating) light, indicating a loss of photoprotective
233 responses; and 4) increased slowly reversible NPQ response (q_I) increased in the mutant,
234 especially later in the day, suggesting the accumulation of photoinhibition.

235 Differences in photosynthesis between SALK_098173 and Col-0 persisted into day 4
236 (**Fig. 3a**), with the mutant showing decreases in maximal PSII quantum yield ($F_v/F_M \sim 0.7$),
237 possibly reflecting accumulation of photoinhibition (but see below), and decreased ϕ_{II} and LEF,
238 particularly in the early morning, possibly reflecting limitations at the photosystems or
239 downstream metabolic processes. The relative loss of maximal quantum efficiency in the mutant
240 had largely recovered on the morning of day 5, but application of fluctuating light during day 5
241 revealed new effects of SALK_098173, most notably a suppression of the q_E response and
242 progressive loss of ϕ_{II} and LEF.

243

244 *Spatial and temporal heterogeneity of dynamic photosynthetic responses in SALK_098173.*

245 Closer examination of the DEPI images revealed that SALK_098173 showed strongly
246 heterogeneous photosynthetic phenotypes that depended on both on leaf development and light

treatment. These heterogeneous responses can be seen in the false-color images taken at selected time points (**Fig. 3**, **Supplemental Fig. 3** and **Supplemental Video 1**), kinetically-resolved plots of individual photosynthetic parameters (**Supplemental Fig. 4**) and in heat maps comparing parameters to the surface-averaged results from Col-0 (**Fig. 4b**). Tissue-dependent differences were also seen in Col-0, but were much more subtle (**Supplemental Fig. 5** and **Supplemental Video 2**). For the purpose of this discussion, the leaves are numbered in pairs according to their developmental ages, i.e. pair 1 for the cotyledon leaves, 2 for the first rosette leaves, 3 for the next oldest rosette leaves and so on.

Photosynthetic parameters in the leaf pair 4 remained nearly indistinguishable in Col-0 and SALK_098173 over the course of the experiment, except for a somewhat elevated q_E response in the mutant during fluctuating light on days 3 and 5. In contrast, the older leaves showed strong phenotypes that appeared at unexpected times after exposure to dynamic light conditions. On day 1, under flat lighting, all leaves on the mutant and Col-0 showed similar, homogeneous photosynthetic behaviors (**Fig. 4b** and **Supplemental Figs. 1 and 2**). Likewise, on day 2, only subtle and spatially homogeneous effects appeared in the mutant towards the end of the day, reflected in weak elevation of NPQ, q_E and q_I (by about 10%). Strong, heterogeneous effects appeared abruptly in the mutant on the morning of day 3, specifically in leaf pair 2 (**Fig. 4**), with strong suppression of ϕ_{II} and elevation of NPQ. (It should be noted that to prevent disturbances, we did not assay fluorescence parameters during the night, but there were no signs of altered photosynthesis at the end of day 2, indicating that the effects appeared some time after exposure). The phenotype was also heterogeneous within each affected leaf, affecting preferentially the outer edges and towards the apices of the affected leaves (**Fig. 4 and Supplemental Video 1**). As a result, the false-color images showed distinct “patches” suggesting that the phenotype was caused by developmental, metabolic or physiological factors that varied across the leaf tissue.

The ϕ_{II} parameter in the mutant gradually recovered throughout the day, and became nearly indistinguishable from Col-0 throughout the rest of the experiment. The day 3 NPQ phenotype in the affected areas was attributable to effects on both q_E and q_I , with the former being especially affected at lower light in the morning and evening. The increased NPQ in the mutant decreased over days 4 and 5, though it did not fully recover, suggesting that the plant was able to partially acclimate in response to the conditions on day 3.

278 Remarkably, very similar transient and heterogeneous phenotypes for ϕ_{II} and NPQ were
279 seen on leaf pair 3, but were shifted later in time by about 24 hours. This general pattern was
280 observed in multiple plants (**Supplemental Fig. 6**) suggesting that the phenotype was triggered
281 by a combination of environmental factors (in this case high/fluctuating light) and the
282 developmental state of the leaf tissues.

283 The increased q_I and decreased ϕ_{II} in the affected areas are consistent with previous
284 suggestion that loss of AT1G71500 decreases the stability of PSII⁴⁴. However, the
285 heterogeneous effects preceded the application of fluctuating light on day 3, implying that they
286 were not directly caused by loss of PSII activity (photoinhibition) incurred during the previous
287 day's exposure to sinusoidal illumination. Indeed, in leaf pair 2, photosynthetic capacity largely
288 recovered over a few hours of illumination in day 3, despite being exposed to fluctuating
289 illumination, which appears inconsistent with a simple role in maintaining PSII integrity. Our
290 results instead suggest that AT1G71500 may control a nocturnal-specific process critical for
291 acclimation, remodeling or repair of the photosynthetic apparatus in response to photoinhibition
292 (see also below).

293

294 *Using DEPI as a high throughput screening platform: insights into development-specific*
295 *acclimation of photosynthesis to light stress.*

296 To demonstrate the high throughput capabilities if DEPI, and to gain further insights into
297 the nature of the emergent “patchy” phenotypes, we screened of a library of more than 300 T-
298 DNA lines from multiple REP experiments as described above. To select the mutants in an
299 unbiased way, we developed and applied an image analysis algorithm (see Supplemental
300 Materials and Methods) that automatically scans DEPI image data and detect heterogeneous
301 photosynthetic phenotypes. The *psb33* (SALK_098173) lines described above were readily
302 detected, demonstrating the ability of the system to detect the general phenomenon. In addition,
303 we found a number of lines with photosynthetic behaviors similar to *psb33*, and describe 12 of
304 these with the strongest phenotypes here (**Supplemental Fig. 7**). Most of these lines showed
305 only weak phenotypes on the flat illumination on day 1 but distinct heterogeneous phenotypes on
306 days 2, 3 or 4 (**Supplemental Table 1**). The mutations associated with these phenotypes affect
307 genes encoding proteins with a range of predicted functions (**Supplemental Table 1**), including
308 PSII stability and antenna state transitions (PsbR), photoprotection (NPQ7), triose-phosphate

309 transport (TPT), and putative transcription factors involved in abiotic stress signaling (e.g.
310 AT3G10470), as well as several genes of unknown functions (At1g16880, At3g46610,
311 At5g59250, At5g08540, At2g29180). Loci for which multiple independent knockout alleles were
312 available, showed similar phenotypes, suggesting that knocking out each of these genes
313 independently was able to induce the phenomenon. Thus, the diversity of the genes involved
314 implies that the phenomenon reflects the effects of multiple interacting processes.

315 While a complete characterization of all the “patchy” mutants is beyond the scope of this
316 work, we were able to apply DEPI to develop and test possible mechanisms. While in all cases,
317 the patchy areas showed decreased Φ_{II} and increased NPQ (both q_E and q_I components) (data for
318 a subset is show in **Fig. 5 and Supplemental Fig. 7**), there was a general trend in which
319 decreased ϕ_{II} and increased q_E appeared very early in the day, whereas q_I tended to accumulate
320 over time (**Supplemental Figs. 8 and 9 and Supplemental Video 3**), suggesting that the
321 mutations initially suppressed photosynthesis by feedback regulation involving the buildup of
322 thylakoid *pmf*, but that q_E was unable to fully protect the photosynthetic apparatus, leading to
323 photoinhibition.

324 One possible mechanism for the observed effects on photosynthesis is decreased stomatal
325 conductance, which will decrease internal CO₂ levels and thus leads to slow ATP synthase and
326 increased *pmf* and q_E responses^{48, 49}. Indeed, stomatal closure has been previously associated
327 with heterogeneous (or patchy) photosynthetic patterns⁵⁰⁻⁵³. We therefore tested if the
328 phenotypes we observed could be reversed under elevated CO₂, which bypasses restrictions to
329 photosynthesis caused by low stomatal conductance. **Supplemental Figures 10 and 11** (and
330 **Supplemental Video 4**) show that responses to CO₂ varied, but none of the lines showed strong
331 suppression of patchy phenotypes, implying that the patchy phenotypes were not caused by
332 altered stomata responses.

333 A subset of the patchy mutants (SALK_098173, WISCD SLOXHS054_06G, *tpt*,
334 SALK_114469, SALK_059367) showed high fluorescence yield in their patchy regions even at
335 very low light intensities. This effect is illustrated for selected mutants for which the effect was
336 strongest (**Fig. 6**), where we illuminated with a series of weakly actinic measuring flashes spaced
337 70 ms in time apart (giving an average light intensity of about 10 $\mu\text{mol photons m}^{-2} \text{s}^{-1}$). In the
338 wild type, and in non-patchy regions of the mutants, only very small changes in fluorescence
339 yield were seen, indicating that Q_A was fully reoxidized between flashes. However, in the patchy

340 regions of the mutants, the fluorescence yield increased monotonically with each successive
341 flash, indicating the accumulation of reduced Q_A^- . Because maximal quantum efficiency for PSII
342 photochemistry in the regions was similar to or less than that of the wild types, this accumulation
343 must have been caused by inhibition of Q_A re-oxidation (rather than an increase in the rate of
344 PSII excitation). The effect was not reversed by application of far red illumination
345 (**Supplemental Fig. 12**), which preferentially excites PSI photochemistry and thus oxidizes
346 plastoquinol, arguing against the possibility that it was caused by reduction of the PQ pool
347 through cyclic electron flow (CEF) or chlororespiration⁵⁴. We thus propose that the high
348 fluorescence level at low light most likely reflects the accumulation of a substantial fraction of
349 PSII centers in non-functional states, perhaps related to the reported upshift in Q_A redox potential
350 that accompanies loss of Ca^{2+} from the oxygen evolving complex⁵⁵ or the occurrence of so-called
351 centers inactive in electron transfer from Q_A to Q_B ^{56, 57}.

352 Regardless of the mechanisms, the appearance of the modified PSII behavior centers did
353 not immediately follow exposure to high light at the end of the previous day (**Supp. Video 1,**
354 **Fig. 4**), implying that the effect cannot be attributed to the immediate effects of photodamage.
355 Instead, the fact that the effects are transitory and precede decreases in sensitivity of
356 photosynthesis to subsequent exposure to fluctuating light, suggests that they reflect the process
357 of “remodeling” the photosynthetic apparatus to acclimate to fluctuating light.

358

359 **Conclusions**

360 By addressing limitations in current technology, the DEPI platform enables direct
361 assessment of rapid and long-term responses of photosynthesis for a large number of plants
362 under diverse but reproducible dynamic environmental conditions. The utility of the DEPI
363 technology was demonstrated by detection of, and subsequent high-throughput screening for,
364 complex phenotypes that would otherwise be extremely difficult to characterize. These
365 phenotypes appear under non-laboratory conditions, are highly transient and are both temporally
366 and spatially heterogeneous and depended in complex ways on genotype, environment and
367 developmental stage. The tight control of environmental conditions and simultaneous imaging of
368 all plants enabled DEPI to observe these behaviors very reproducibly (**Figs. 2-4**), and thus to
369 study in detail phenomena relevant to natural or agricultural conditions.

370 We followed up in some detail on the peculiar “patchy” phenotypes that appeared in a
371 set of mutants following fluctuating light, partly because this type of phenomenon has not to our
372 knowledge been reported, and also because it allowed us to demonstrate some of the advanced
373 capabilities of the DEPI platform. These effects appeared some time after exposure to high and
374 fluctuating light (**Fig. 5** and **Supp. Fig. 7**), so that they would not have normally been observed
375 in photoinhibition experiments. The time delay also suggests that they are not directly caused by
376 the initial photoinhibition processes, but could be related to slower repair or remodeling of
377 photosynthesis, that leads to acclimation, as suggested by the fact that these regions appear less
378 sensitive to subsequent fluctuating light treatments (see for example leaf-specific phenotypes on
379 days 3 and 5 in **Fig. 3**).

380 While a detailed mechanistic characterization of these mutants (currently on-going) is
381 beyond the scope of this demonstration paper, analysis of various chlorophyll fluorescence
382 parameters led us to propose that the effects are related to formation of a fraction of PSII centers
383 defective in Q_A^- re-oxidation (**Fig. 6**), possibly related to damage to the PSII Q_B site⁵⁷ or oxygen
384 evolving complex, which affects Q_A redox potential⁵⁵ or to disassembly and reassembly of PSII
385 centers^{58, 59}.

386 The diversity of the T-DNA lines displaying patchy phenotypes (SI Table 1) suggests the
387 involvement of a range of different processes that possibly act both directly and indirectly. Some
388 of the genes are proposed to function directly in the light reactions of photosynthesis. For
389 examples, both Psb33 (SALK_098173)⁴⁴ and PsbR (SALK_114469)⁶⁰ have been proposed to be
390 involved in PSII stability and repair cycles and become important under conditions where high
391 rates of damage occur. Similarly, NPQ7 is a chloroplast localized YCF20-like gene involved in
392 nonphotochemical quenching, though its mechanism is not yet understood⁶¹. In contrast, TPT is a
393 transporter in the chloroplast inner envelope⁶² and NDF6 (SALK_056498) is a putative
394 membrane protein that has been proposed to be essential for NDH assembly/activity⁶³. Both of
395 these proteins probably impact PSII reactions indirectly, possibly by affecting metabolic status,
396 leading to alterations in redox status or retrograde signals^{64, 65}. Similarly, the thylakoid ATP/ADP
397 carrier (SALK_119779)⁶⁶, or TAAC, which is proposed to supply the lumen with ATP required
398 for the repair cycle, may also influence stromal ATP/ADP ratio, which in turn can modulate ATP
399 synthase activity⁶⁷. More recent work suggests that TAAC may also function in the chloroplast

400 envelope as a transporter for plastidic phosphoadenosine phosphosulfate (PAPS), and thus may
401 be critical for plastid sulfur metabolism.⁶⁸

402 In conclusion, we demonstrate that DEPI is a useful platform for focusing biochemical,
403 gene expression and physiological studies and ultimately for connecting genome to phenotype.
404 While the current work concentrates on light intensity changes, the DEPI platform can readily be
405 extended to reproduce changes in other environmental parameters, e.g. temperature, humidity
406 soil moisture and nutrient levels. Therefore, it is possible to systematically alter parameters,
407 individually or in combination, to reveal a range of responses to distinct environmental
408 combinations that mimic those experienced in the field. The DEPI is also highly modular and can
409 easily be expanded to fit even large growth facilities for dynamic phenotyping of larger crop
410 plants, as an integral part of new approaches to plant improvement.

411

412 Acknowledgements

413 This work was supported by the U.S. Department of Energy (DOE), Office of Science,
414 Basic Energy Sciences (BES) under Award number DE-FG02-91ER20021 and the MSU Center
415 for Advanced Algal and Plant Phenotyping (CAAPP).

416

417 Online Methods

418

419 *Plants and growth conditions.* Wild type (Col-0) and T-DNA insertion mutants of
420 Arabidopsis were grown at 21°C, 16 hr:8 hr day night cycle, 100 µmol photons m⁻² s⁻¹. Three-
421 week-old plants were transferred to imaging chambers and allowed to acclimate for 24 hours to
422 the LED lighting before the start of the experiments. Homozygous seed lines for SALK_098173
423 (Rieske type Fe-S protein, At1g71500), SAIL_115_E08 (NADPH-dependent thioredoxin
424 reductase, At2g41680), and SALK_103895 (NFU domain protein 3, At4g25910) were obtained
425 from the Chloroplast 2010 Project⁴⁰.

426

427 Design and Construction of DEPI

428 As illustrated in **Figure 1** and **Supplemental Figures 13-14**, DEPI was designed to
429 control key environmental parameters including temperature, humidity and illumination with

430 white (growth) light at intensities and dynamics found in natural environments. DEPI allows
431 sensitive imaging of chlorophyll fluorescence parameters without moving plants or cameras.
432

433 *DEPI Actinic Lighting.* White actinic illumination was provided by 50W Bridgelux White
434 LED arrays (BXRA-56C5300, Bridgelux Inc., Livermore, California) mounted in low thermal
435 resistance heat sinks (North American Extrusions, Heat Sink Profile 79000, Aavid Thermalloy,
436 Laconia, New Hampshire) and arranged in 9 cm (center to center) square grids (**Fig. 1a**). The
437 illumination system is scalable to even large matrices. Banks of 48 LEDs (6 X 8) were used in
438 small prototype systems, and tiles of larger banks containing 156 LEDs (6 X 26) were used in the
439 current imaging system assembled inside an environmentally-controlled plant growth chamber
440 (BioChambers Bigfoot FLXC-19, with base dimensions of 0.76 by 2.46 m, BioChambers,
441 Winnipeg, Manitoba, Canada) modified to accommodate the DEPI lighting, sensors and control
442 circuits and software. Output light intensity was regulated by a master computer through an I²C
443 serial electronic control bus, as described in more detail in **Supplemental Figure 13**, a technical
444 schematic showing integration of power and control systems with LED and camera arrays. To
445 minimize edge effects, LED lighting was controlled in 16 individual zones which were calibrated
446 to maintain even illumination. Saturating illumination required for measurement of certain
447 chlorophyll fluorescence parameters was achieved by pulsing the LED arrays for 0.3s at high
448 current using supplementary lead acid battery power. LEDs were fitted with collimating optics
449 (Britney-M Reflector, LEDIL, Inc., Salo, Finland) to increase intensity at leaf surface and to
450 better simulate solar irradiance. Illumination intensities were measured using a quantum sensor
451 (Licor, Inc. Lincoln, Nebraska). The current imaging systems can achieve continuous
452 illumination intensities at about 5° dispersion in excess of full sunlight (>2,500 µmol photons m⁻²
453 s⁻¹) with 0.5 s saturation pulse intensities in excess of 15,000 µmol photons m⁻² s⁻¹, at a distance
454 of 0.5 m from the light sources. Intensities varied by less than 3% across the planting region. For
455 some experiments far red illumination was supplied by an array of 730 nm LEDs (ELSH-Q61F1-
456 0LPNM-JF3F8, Everlight Electronics Co Ltd, Taipei, Taiwan).

457

458 *DEPI probe illumination.* Light pulses for measuring chlorophyll parameters were
459 provided by a matrix of red-emitting LEDs (Luxeon Rebel SMT High Power LED Red, LXM2-
460 PD01-0050, Philips Lumiled, San Jose, California) with collimating optics (LEDIL

461 FA10993_LISA2-W-PIN-RE, LEDIL Inc., Salo, Finland, reflector or Dialight OPC1-2-COL
462 reflector, Dialight, Suffolk, England). The LEDs were distributed throughout the chamber to
463 achieve even probe illumination (**Figure 1a**). Probe LEDs were pulsed (10-50 μ s duration)
464 through a rapid gating circuit (**Supplemental Fig. 13**) to provide high sensitivity and time
465 resolution but low integrated incident radiation.

466

467 *DEPI Cameras.* Images of chlorophyll fluorescence were captured using high resolution,
468 monochrome CCD cameras with extended near infrared (nIR) sensitivity (KPV145MC, Hitachi,
469 Chiyoda, Japan), outfitted a low distortion, 8mm focal length, 2 megapixel C-mount lens
470 (LM8JCM, Kowa Optical Products, Japan) and with an optical filter that blocks visible light but
471 passes nIR light (Hoya RT830 or Schott RG9, Edmund Optical). By synchronizing LED pulses
472 and image capture across multiple arrays, DEPI can image large populations without moving
473 plants or cameras. This feature also allows DEPI to be readily scalable to larger settings. The
474 current version incorporated an array of 5 cameras in a single chamber.

475 Image capture was triggered during a ~100 μ s dark interval during which actinic or
476 saturating light was electronically shuttered (**Supplemental Fig. 14**). The measuring pulse
477 occurred 10-35 μ s after switching off the actinic light. Systematically varying the timing showed
478 that this delay was sufficiently short to prevent substantial decay of fluorescence properties. The
479 rise in fluorescence induced by a series of measuring pulses in dark-adapted leaves, as described
480 in Kramer et al.⁶⁹, shows that each measuring pulse excited less than 1% of photosystem II
481 centers. This measurement method yields estimates of relative chlorophyll fluorescence yield
482 because pulse-to-pulse intensities, camera gain settings and optical filter combinations are held
483 constant. Also, by eliminating spectral contamination of chlorophyll fluorescence in the near
484 infrared by actinic illumination, the method allows measurements under arbitrary light quality
485 actinic illumination, including especially the white light used for growth.

486

487 *DEPI controller and software.* Control software was developed in the JAVA language
488 (Netbeans 7.3, www.netbeans.org) with supplemental code developed in Visual C++ (Microsoft
489 Visual Studio 2010), using drivers/libraries/SDKs provided by the camera manufacturer. Signals
490 for setting light intensity, gating actinic light, gating the saturation pulse, controlling measuring
491 pulses and triggering cameras (**Supplemental Fig. 13**) were generated by a 50 MHz resolution

492 digital programmable timer by programming a field-programmable gate array (FPGA, Nexsys-2,
493 Digilent) using the Verilog language (<http://www.verilog.com/>).

494

495 *Image Processing and Analysis.* Image capture protocols were patterned to measure
496 standard saturation pulse chlorophyll fluorescence parameters, as reviewed in Baker et al.^{18 17}.
497 Images were captured before, during and after the application of saturating actinic pulses.
498 Typically 5 frames for each phase (15 frames total) were collected with a 60 ms delay between
499 images. Corrections were applied to account for artifacts caused by residual electrons in the CCD
500 array that occurred during saturation pulse exposure. These sequences of images were collected
501 before the beginning of each daylight cycle (F_0 , F_M , in the absence or presence of saturating
502 actinic light, respectively) as well as immediately before (F_s , F_M' , in the absence or presence of
503 saturating actinic light, respectively) and at the end of each 2 min dark period (F_M'' , in presence
504 of saturating actinic light). Images sequences were used to calculate the quantum yield of
505 photosynthesis of PSII (Φ_{II}), non-photochemical quenching (NPQ), energy dependent quenching
506 (q_E) and slowly reversible inhibitory quenching (q_I), which may reflect both photoinhibition¹⁷
507 and movements of chloroplasts³⁵.

508 Data analysis was performed using software developed in-house based on the open
509 source software resources, ImageJ (<http://rsbweb.nih.gov/ij/>)⁷⁰ and Netbeans 7.3
510 (www.netbeans.org), and will be described in detail in a separate publication. The package
511 allows calculation and visualization of photosynthetic parameters across selected regions of
512 interest and over variable time ranges.

513 To detect “patchy” phenotypes an algorithm was designed to flag mutants in which Φ_{II}
514 variance was high. Pixels for each plant were binned based on intensity. Absolute range was
515 calculated from the minimum and maximum pixel intensities after exclusion of the upper
516 (highest intensities) and lower (lowest intensities) 2 percent of the population. Ranges were
517 normalized to the mean intensities to bias the selection for plants where Φ_{II} decreases
518 dramatically. From this pool of candidates (which included 20 to 30 lines) patchiness was
519 confirmed by visual examination of the images in 9 lines.

520

521 **References**

522

- 523 1. Raven, J.A. The cost of photoinhibition. *Physiol. Plant.* **142**, 87-104 (2011).
- 524 2. Murchie, E.H. & Niyogi, K.K. Manipulation of photoprotection to improve plant
525 photosynthesis. *Plant Physiol.* **155**, 86-92 (2011).
- 526 3. Kramer, D.M. & Evans, J.R. The importance of energy balance in improving
527 photosynthetic productivity. *Plant Physiol.* **155**, 70-78 (2011).
- 528 4. Suorsa, M. et al. PROTON GRADIENT REGULATION5 is essential for proper
529 acclimation of *Arabidopsis* photosystem I to naturally and artificially fluctuating light
530 conditions. *Plant Cell* **24**, 2934-2948 (2012).
- 531 5. Tikkkanen, M. et al. Regulation of the photosynthetic apparatus under fluctuating growth
532 light. *Philos. Trans. R. Soc. B* **367**, 3486-3493 (2012).
- 533 6. Rascher, U. & Nedbal, L. Dynamics of photosynthesis in fluctuating light. *Curr. Opin.*
534 *Plant Biol.* **9**, 671-678 (2006).
- 535 7. Blankenship, R.E. et al. Comparing photosynthetic and photovoltaic efficiencies and
536 recognizing the potential for improvement. *Science* **332**, 805-809 (2011).
- 537 8. Zhu, X.G., Long, S.P. & Ort, D.R. Improving photosynthetic efficiency for greater yield.
538 *Annu. Rev. Plant Biol.* **61**, 235-261 (2010).
- 539 9. Boyer, J.S. Plant productivity and environment. *Sci.* **218**, 443-448 (1982).
- 540 10. Vadez, V. et al. Adaptation of grain legumes to climate change: a review. *Agron. Sustain.*
541 *Dev.* **32**, 31-44 (2012).
- 542 11. Gaspar, T. et al. Concepts in plant stress physiology. Application to plant tissue cultures.
543 *Plant Growth Regul.* **37**, 263-285 (2002).
- 544 12. Kulheim, C., Agren, J. & Jansson, S. Rapid regulation of light harvesting and plant
545 fitness in the field. *Science* **297**, 91-93 (2002).
- 546 13. Grieco, M., Tikkkanen, M., Paakkarinen, V., Kangasjarvi, S. & Aro, E.M. Steady-state
547 phosphorylation of light-harvesting complex II proteins preserves photosystem I under
548 fluctuating white light. *Plant Physiol.* **160**, 1896-1910 (2012).
- 549 14. Mishra, Y. et al. *Arabidopsis* plants grown in the field and climate chambers significantly
550 differ in leaf morphology and photosystem components. *BMC Plant Biol.* **12**, 6 (2012).
- 551 15. Munns, R., James, R.A., Sirault, X.R.R., Furbank, R.T. & Jones, H.G. New phenotyping
552 methods for screening wheat and barley for beneficial responses to water deficit. *J. Exp.*
553 *Bot.* **61**, 3499-3507 (2010).
- 554 16. Long, S.P. & Bernacchi, C.J. Gas exchange measurements, what can they tell us about
555 the underlying limitations to photosynthesis? Procedures and sources of error. *J. Exp.*
556 *Bot.* **54**, 2393-2401 (2003).
- 557 17. Baker, N.R. & Oxborough, K. in *Chlorophyll a fluorescence: a signature of*
558 *photosynthesis*. (eds. G.C. Papageorgiou & Govindjee) 65–82 (Springer, Dordrecht, the
559 Netherlands; 2004).
- 560 18. Baker, N.R., Harbinson, J. & Kramer, D.M. Determining the limitations and regulation of
561 photosynthetic energy transduction in leaves. *Plant Cell Environ.* **30**, 1107-1125 (2007).
- 562 19. Kramer, D.M. & Crofts, A.R. in *Photosynthesis and the environment*. (ed. N.R. Baker)
563 25-66 (Kluwer Academic Press, Dordrecht, The Netherlands; 1996).
- 564 20. Omasa, K., Hosoi, F. & Konishi, A. 3D lidar imaging for detecting and understanding
565 plant responses and canopy structure. *J. Exp. Bot.* **58**, 881-898 (2007).
- 566 21. Paproki, A., Sirault, X., Berry, S., Furbank, R. & Fripp, J. A novel mesh processing based
567 technique for 3D plant analysis. *BMC Plant Biol.* **12**, 63 (2012).

- 568 22. Sirault, X.R.R., James, R.A. & Furbank, R.T. A new screening method for osmotic
569 component of salinity tolerance in cereals using infrared thermography. *Funct. Plant*
570 *Biol.* **36**, 970-977 (2009).
- 571 23. Stroppiana, D., Boschetti, M., Brivio, P.A. & Bocchi, S. Plant nitrogen concentration in
572 paddy rice from field canopy hyperspectral radiometry. *Field Crops Res.* **111**, 119-129
573 (2009).
- 574 24. Roy, S.J., Tucker, E.J. & Tester, M. Genetic analysis of abiotic stress tolerance in crops.
575 *Curr. Opin. Plant Biol.* **14**, 232-239 (2011).
- 576 25. Morgan, D.C. & Smith, H. Control of development in *Chenopodium Album L.* by
577 shadelight: The effect of light quantity (total fluence rate) and light quality (red.far-red
578 ratio) *New Phytol.* **88**, 239-248 (1981).
- 579 26. Braam, J. & Davis, R.W. Rain-, wind-, and touch-induced expression of calmodulin and
580 calmodulin-related genes in *Arabidopsis*. *Cell* **60**, 357-364 (1990).
- 581 27. Braam, J. In touch: plant responses to mechanical stimuli. *New Phytol.* **165**, 373-389
582 (2005).
- 583 28. Singsaas, E.L. & Sharkey, T.D. The regulation of isoprene emission responses to rapid
584 leaf temperature fluctuations. *Plant, Cell Environ.* **21**, 1181-1188 (1998).
- 585 29. Schäufele, R., Santrucek, J. & Schnyder, H. Dynamic changes of canopy-scale mesophyll
586 conductance to CO₂ diffusion of sunflower as affected by CO₂ concentration and
587 abscisic acid. *Plant, Cell Environ.* **34**, 127-136 (2011).
- 588 30. Poorter, H. et al. Biomass allocation to leaves, stems and roots: meta-analyses of
589 interspecific variation and environmental control. *New Phytol.* **193**, 30-50 (2012).
- 590 31. Nedbal, L. & Whitmarsh, J. in *Chlorophyll a fluorescence: a signature of photosynthesis*,
591 Vol. 19. (eds. C. Papaeorgio & Govindjee) 389-407 (Kluwer Academic Publishers,
592 Dordrecht, The Netherlands; 2004).
- 593 32. Oxborough, K. Imaging of chlorophyll a fluorescence: theoretical and practical aspects of
594 an emerging technique for the monitoring of photosynthetic performance. *J. Exp. Bot.* **55**,
595 1195-1205 (2004).
- 596 33. Oxborough, K. in *Chlorophyll a fluorescence: a signature of photosynthesis*, Vol. 19.
597 (eds. G. Papageorgiou & Govindjee) 409-428 (Springer Netherlands, 2004).
- 598 34. White, J.W. et al. Field-based phenomics for plant genetics research. *Field Crops Res.*
599 **133**, 101-112 (2012).
- 600 35. Cazzaniga, S., Dall' Osto, L., Kong, S.-G., Wada, M. & Bassi, R. Interaction between
601 avoidance of photon absorption, excess energy dissipation and zeaxanthin synthesis
602 against photooxidative stress in *Arabidopsis*. *The Plant Journal* **76**, 568-579 (2013).
- 603 36. Horton, P. & Hague, A. Studies on the induction of chlorophyll fluorescence in isolated
604 barley protoplasts. IV. Resolution of non-photochemical quenching. *Biochim. Biophys.*
605 *Acta* **932**, 107-115 (1988).
- 606 37. Nilkens, M. et al. Identification of a slowly inducible zeaxanthin-dependent component
607 of non-photochemical quenching of chlorophyll fluorescence generated under steady-
608 state conditions in *Arabidopsis*. *Biochim. Biophys. Acta* **1797**, 466-475 (2010).
- 609 38. Dutta, S. et al. Non-invasive, whole-plant imaging of chloroplast movement and
610 chlorophyll fluorescence reveals photosynthetic phenotypes independent of chloroplast
611 photorelocation defects in chloroplast division mutants. *Plant J.* **84**, 428-442 (2015).

- 612 39. Baker, N.R., Oxborough, K., Lawson, T. & Morison, J.I.L. High resolution imaging of
613 photosynthetic activities of tissues, cells and chloroplasts in leaves. *J. Exp. Bot.* **52**, 615-
614 621 (2001).
- 615 40. Lu, Y., Savage, L.J., Larson, M.D., Wilkerson, C.G. & Last, R.L. Chloroplast 2010: a
616 database for large-scale phenotypic screening of *Arabidopsis* mutants. *Plant Physiol.* **155**,
617 1589-1600 (2011).
- 618 41. Ajjawi, I., Lu, Y., Savage, L.J., Bell, S.M. & Last, R.L. Large-scale reverse genetics in
619 *Arabidopsis*: case studies from the Chloroplast 2010 Project. *Plant Physiol.* **152**, 529-540
620 (2010).
- 621 42. Peltier, J.B., Ytterberg, A.J., Sun, Q. & van Wijk, K.J. New functions of the thylakoid
622 membrane proteome of *Arabidopsis thaliana* revealed by a simple, fast, and versatile
623 fractionation strategy. *J. Biol. Chem.* **279**, 49367-49383 (2004).
- 624 43. Friso, G. et al. In-depth analysis of the thylakoid membrane proteome of *Arabidopsis*
625 *thaliana* chloroplasts: new proteins, new functions, and a plastid proteome database. *Plant*
626 *Cell* **16**, 478-499 (2004).
- 627 44. Fristedt, R. et al. PHOTOSYSTEM II PROTEIN33, a protein conserved in the plastid
628 lineage, is associated with the chloroplast thylakoid membrane and provides stability to
629 photosystem II supercomplexes in *Arabidopsis*. *Plant Physiol.* **167**, 481-492 (2015).
- 630 45. Takizawa, K., Cruz, J.A., Kanazawa, A. & Kramer, D.M. The thylakoid proton motive
631 force in vivo. Quantitative, non-invasive probes, energetics, and regulatory consequences
632 of light-induced pmf. *Biochim. Biophys. Acta* **1767**, 1233-1244 (2007).
- 633 46. Müller, P., Li, X.P. & Niyogi, K.K. Non-photochemical quenching. A response to excess
634 light energy. *Plant Physiol.* **125**, 1558-1566 (2001).
- 635 47. Dutta, S. et al. Non-invasive, whole-plant imaging of chloroplast movement and
636 chlorophyll fluorescence reveals photosynthetic phenotypes independent of chloroplast
637 photorelocation defects in chloroplast division mutants. *The Plant Journal* **84**, 428-442
638 (2015).
- 639 48. Kohzuma, K. et al. Thioredoxin-insensitive plastid ATP synthase that performs
640 moonlighting functions. *Proc Natl Acad Sci U S A* **109**, 3293-3298 (2012).
- 641 49. Kanazawa, A. & Kramer, D.M. In vivo modulation of nonphotochemical exciton
642 quenching (NPQ) by regulation of the chloroplast ATP synthase. *Proc Natl Acad Sci U S*
643 *A* **99**, 12789-12794 (2002).
- 644 50. Lawson, T., Weyers, J. & A'Brook, R. The nature of heterogeneity in the stomatal
645 behaviour of *Phaseolus vulgaris* L. primary leaves. *J. Exp. Bot.* **49**, 1387-1395 (1998).
- 646 51. Loreto, F. & Sharkey, T.D. Low humidity can cause uneven photosynthesis in olive (*Olea*
647 *europea* L.) leaves. *Tree Physiol.* **6**, 409-415 (1990).
- 648 52. Mott, K.A. & Buckley, T.N. Stomatal heterogeneity. *J. Exp. Bot.* **49**, 407-417 (1998).
- 649 53. Attaran, E. et al. Temporal Dynamics of Growth and Photosynthesis Suppression in
650 Response to Jasmonate Signaling. *Plant Physiol.* **165**, 1302-1314 (2014).
- 651 54. Strand, D.D. et al. Activation of cyclic electron flow by hydrogen peroxide in vivo. *Proc.*
652 *Natl. Acad. Sci. USA* **112**, 5539-5544 (2015).
- 653 55. Krieger, A. & Rutherford, A.W. Comparison of chloride-depleted and calcium-depleted
654 PSII: the midpoint potential of QA and susceptibility to photodamage. *Biochim. Biophys.*
655 *Acta* **1319**, 91-98 (1997).

- 656 56. Chylla, R.A., Garab, G. & Whitmarsh, J. Evidence for slow turnover in a fraction of
657 Photosystem II complexes in thylakoid membranes. *Biochim. Biophys. Acta* **894**, 562-571
658 (1987).
- 659 57. Chylla, R.A. & Whitmarsh, J. Inactive Photosystem II Complexes in Leaves : Turnover
660 Rate and Quantitation. *Plant Physiol.* **90**, 765-772 (1989).
- 661 58. Nath, K. et al. Towards a critical understanding of the photosystem II repair mechanism
662 and its regulation during stress conditions. *FEBS Lett.* **587**, 3372-3381 (2013).
- 663 59. Belgio, E., Johnson, Matthew P., Jurić, S. & Ruban, Alexander V. Higher Plant
664 Photosystem II Light-Harvesting Antenna, Not the Reaction Center, Determines the
665 Excited-State Lifetime—Both the Maximum and the Nonphotochemically Quenched.
Biophys. J. **102**, 2761-2771 (2012).
- 666 60. Liu, H., Frankel, L.K. & Bricker, T.M. Characterization and complementation of a psbR
667 mutant in Arabidopsis thaliana. *Arch. Biochem. Biophys.* **489**, 34-40 (2009).
- 668 61. Jung, H.-S. & Niyogi, K. Mutations in Arabidopsis YCF20-like genes affect thermal
669 dissipation of excess absorbed light energy. *Planta* **231**, 923-937 (2010).
- 670 62. Schneider, A. et al. An Arabidopsis thaliana knock-out mutant of the chloroplast triose
671 phosphate/phosphate translocator is severely compromised only when starch synthesis,
672 but not starch mobilisation is abolished. *Plant J.* **32**, 685-699 (2002).
- 673 63. Ishikawa, N. et al. NDF6: a thylakoid protein specific to terrestrial plants is essential for
674 activity of chloroplastic NAD(P)H dehydrogenase in Arabidopsis. *Plant Cell Physiol.* **49**,
675 1066-1073 (2008).
- 676 64. Rolland, F., Baena-Gonzalez, E. & Sheen, J. SUGAR SENSING AND SIGNALING IN
677 PLANTS: Conserved and Novel Mechanisms. *Annu. Rev. Plant Biol.* **57**, 675-709 (2006).
- 678 65. Sharkey, T.D., Laporte, M., Lu, Y., Weise, S. & Weber, A.P.M. Engineering Plants for
679 Elevated CO₂: A Relationship between Starch Degradation and Sugar Sensing. *Plant
680 Biol.* **6**, 280-288 (2004).
- 681 66. Thuswaldner, S. et al. Identification, expression, and functional analyses of a thylakoid
682 ATP/ADP carrier from Arabidopsis. *J. Biol. Chem.* **282**, 8848-8859 (2007).
- 683 67. Yin, L. et al. Role of Thylakoid ATP/ADP Carrier in Photoinhibition and Photoprotection
684 of Photosystem II in Arabidopsis. *Plant Physiol.* **153**, 666-677 (2010).
- 685 68. Gigolashvili, T. et al. The Arabidopsis Thylakoid ADP/ATP Carrier TAAC Has an
686 Additional Role in Supplying Plastidic Phosphoadenosine 5'-Phosphosulfate to the
687 Cytosol. *The Plant Cell* **24**, 4187-4204 (2012).
- 688 69. Kramer, D.M., Robinson, H.R. & Crofts, A.R. A portable multi-flash kinetic fluorimeter
689 for measurement of donor and acceptor reactions of photosystem 2 in leaves of intact
690 plants under field conditions. *Photosynthesis Res.* **26**, 181-193 (1990).
- 691 70. Schneider, C.A., Rasband, W.S. & Eliceiri, K.W. NIH Image to ImageJ: 25 years of
692 image analysis. *Nat Meth* **9**, 671-675 (2012).
- 693
- 694
- 695

696 **Figure 1. Tracking photosynthetic performance using DEPI under ramped environmental
697 perturbations (REP).** Plants were grown and photosynthetic performance was monitored in a
698 DEPI chamber (**a**) over 5 days of light intensity ramped environmental perturbations (**b**)
699 sequentially going through a flat day (day 1), a sinusoidal day (day 2), a fluctuating day (day 3),

700 a flat day (day 4) and finally a fluctuating day (day 5), as described in Results. A period of
701 complete darkness was required to estimate the q_E and q_I parameters; to avoid perturbations, the
702 frequency of these measurements (at the end of every hour on flat days, or the end of each
703 intensity change on sinusoidal and fluctuating days) and the duration of the dark period (2 min)
704 were kept to a minimum. More extensive follow up experiments were performed to assess the
705 accuracy of these estimates.

706

707 **Figure 2. High throughput measurements of photosynthetic parameters using DEPI.**

708 Composite images of Φ_{II} (**a**) and q_E (**b**) stitched from 5 camera views for 231 plants
709 encompassing 52 mutant lines with wild type controls captured at the beginning of a fluctuating
710 day, (intensity $40 \mu\text{mol photons m}^{-2} \text{ sec}^{-1}$). Enclosed in squares are plants for mutant lines
711 SALK_103895 (NFU domain protein 3, At4g25910, yellow), SAIL_115_E08 (NADPH-
712 dependent thioredoxin reductase, At2g41680, red) and SALK_098173 (PSB33, At1g71500,
713 blue) and in circles wild type, (*col-0*), referred to in the Results section as SALK_103895,
714 SAIL_115_E08 and SALK_098173, respectively. Averaged Φ_{II} (**c**, red) and q_E (**d**, gray) values
715 for are shown in bar graphs ($n=4$) with representative images from panels **a** and **b** displayed
716 below each bar.

717

718

719 **Figure 3. Emergent phenotypes in SALK_098173, a T-DNA mutant affecting a gene of**
720 **unknown function.** Daily light intensity changes occurring over a 5-day period are shown with
721 corresponding averaged ($n=4$) photosynthetic parameters (Φ_{II} , LEF, NPQ, q_E and q_I) for wild
722 type (Col-0, *red*) and SALK_098173 (SALK_098173, *black*), with standard deviations
723 represented by the shaded areas. Dashed magenta (Col-0) and cyan (SALK_098173) lines in the
724 plots of Φ_{II} indicate averaged F_V/F_M values. For clarity, expanded views of days 3 and 5 are
725 presented in Supplemental Figure 3.

726

727 **Figure 4. Spatial and temporal heterogeneity of photosynthetic performance in**
728 **SALK_098173.** False color images (**a**) of Φ_{II} collected early in the day are shown for a
729 SALK_098173 plant on each of measurement with arrows pointing towards specific leaf pairs as
730 described in Results: cotyledons (yellow, *leaf 1*) first rosette leaves (grey, *leaf 2*), second rosette

731 leaves (green, *leaf 3*) and third rosette leaves (magenta, *leaf 4*). **(b)** Heat maps show fold changes
732 over Col-0 in the averaged photosynthetic parameters (Φ_{II} , NPQ, q_E and q_I) of SALK_098173
733 (Avg.) from **Figure 3b** with heat maps for parameters obtained sampling *leaves 2, 3 and 4*.
734 Green and magenta indicate values lower and greater than the surface averaged Col-0,
735 respectively.

736

737

738 **Figure 5. Identification of other mutants with “patchy” phenotypes.** False color images of
739 F_v/F_M and of Φ_{II} , NPQ, q_E and q_I after **(a)** ~2 hours of actinic illumination on day 3 for *Col-0*,
740 *tpt*, WISCDLOXHS054_06G (ACT domain containing protein) and SALK_059367
741 (Pentatricopeptide repeat superfamily protein) and **(b)** ~1 hour of illumination on day 4, for *Col-*
742 *0*, SALK_098173 (*psb33-1*) and SALK_114469 (*PsbR*).

743

744

745 **Figure 6. Heterophenotypic regions show altered PSII activity.** *Panel a* shows the
746 fluorescence values for the high ‘ F_0 ’ (open symbols) and low ‘ F_0 ’ (closed symbols) regions of
747 individual plants on day 3 for *Col-0* (black, n=3), *tpt* (red, n=5), WISCDLOXHS054_06G
748 (green, n=5) and SALK_206346 (blue, n=5) from 15 sequential frames, each given a partially
749 actinic measuring flash. *Panel b* shows the same for *Col-0* (black, n=5), SALK_098173 (red,
750 n=4), *tpt* (green, n=4), and SALK_114469 (blue, n=5), on day 4. Images were collected every
751 70 ms, allowing QA^- in active PSII centers to be reoxidized. Individual traces for each line were
752 normalized to the values of the first measuring pulse, estimated to be near the fully dark-adapted
753 value, F_0 . To the right of each panel are representative false color images of dark-adapted (‘ F_0 ’,
754 Frame 1) and the weak-light induced fluorescence yield (Frame 15) for *Col-0*, *tpt*,
755 WISCDLOXHS054_06G from *panel a* and *Col-0*, SALK_098173, *tpt*, and SALK_114469
756 from *panel b* (top to bottom).

757

Figure 1

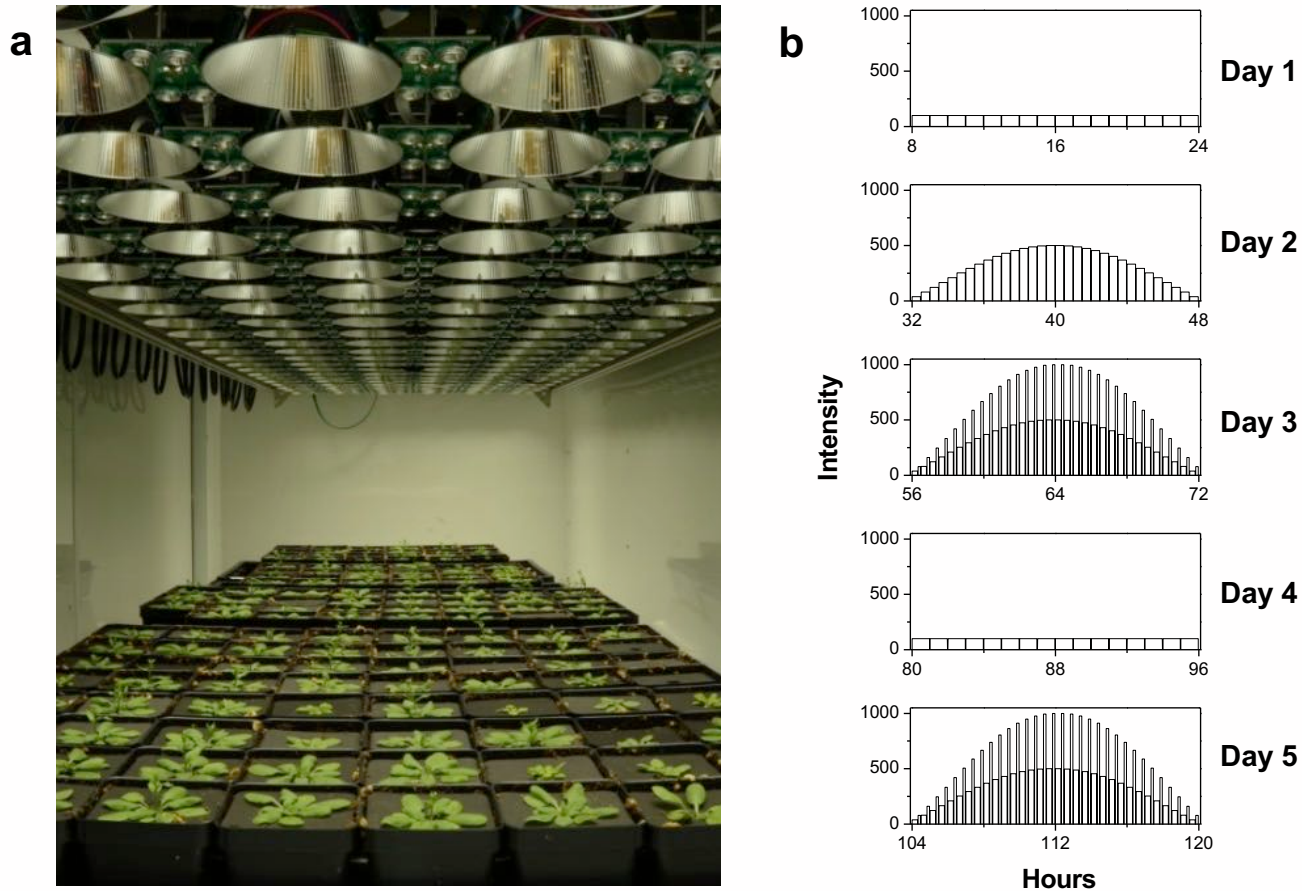


Figure 2

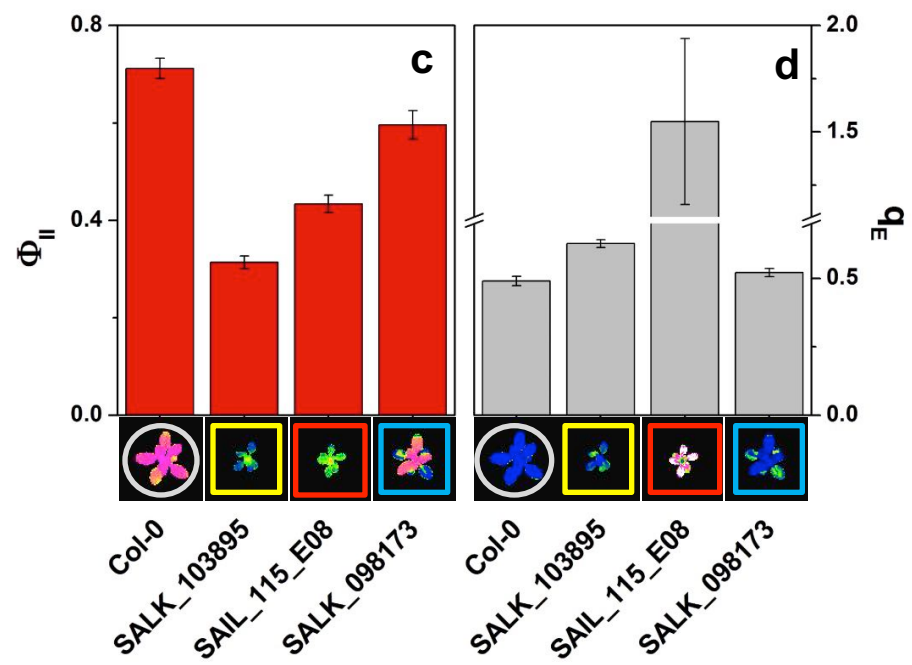
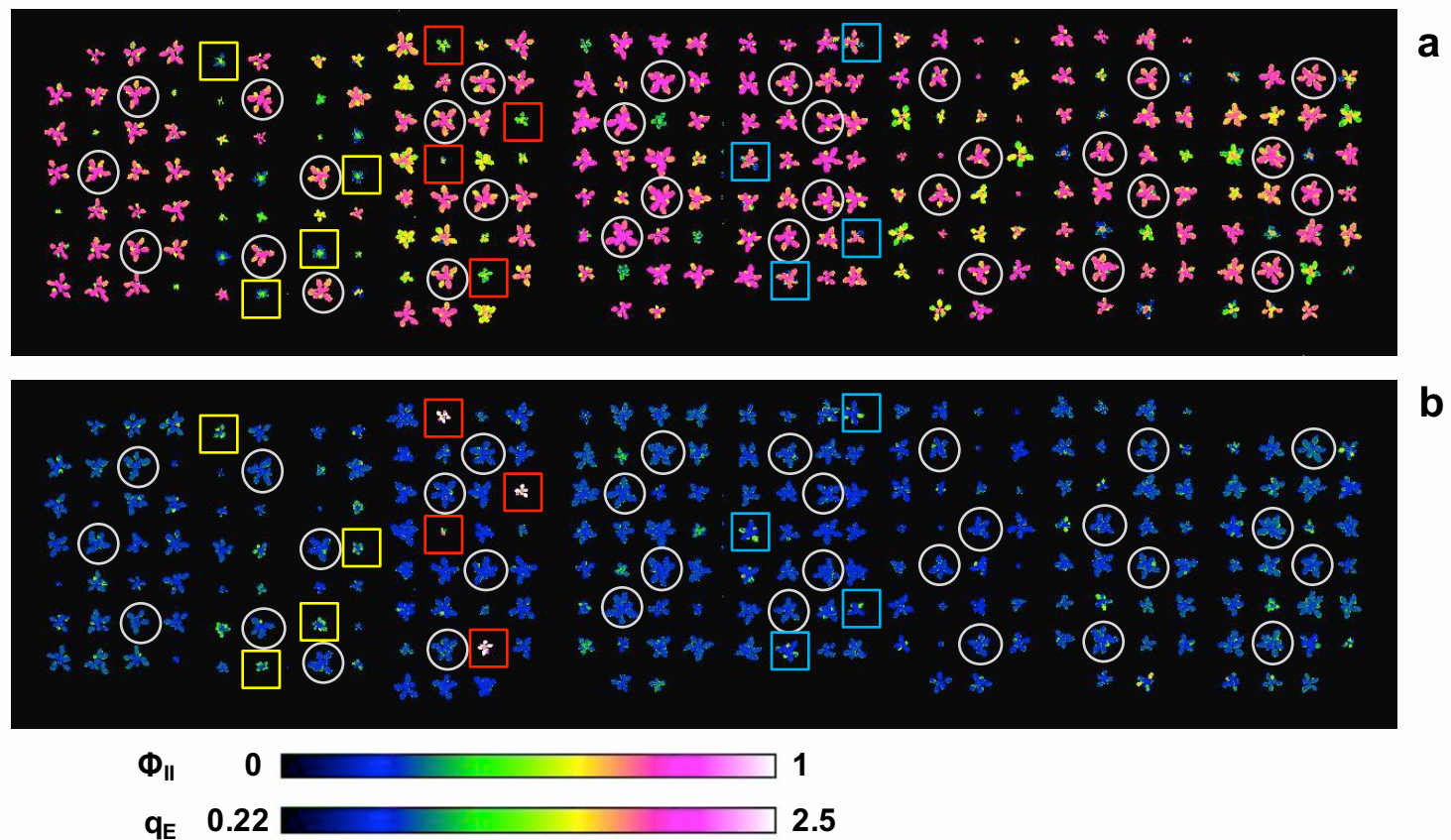


Figure 3

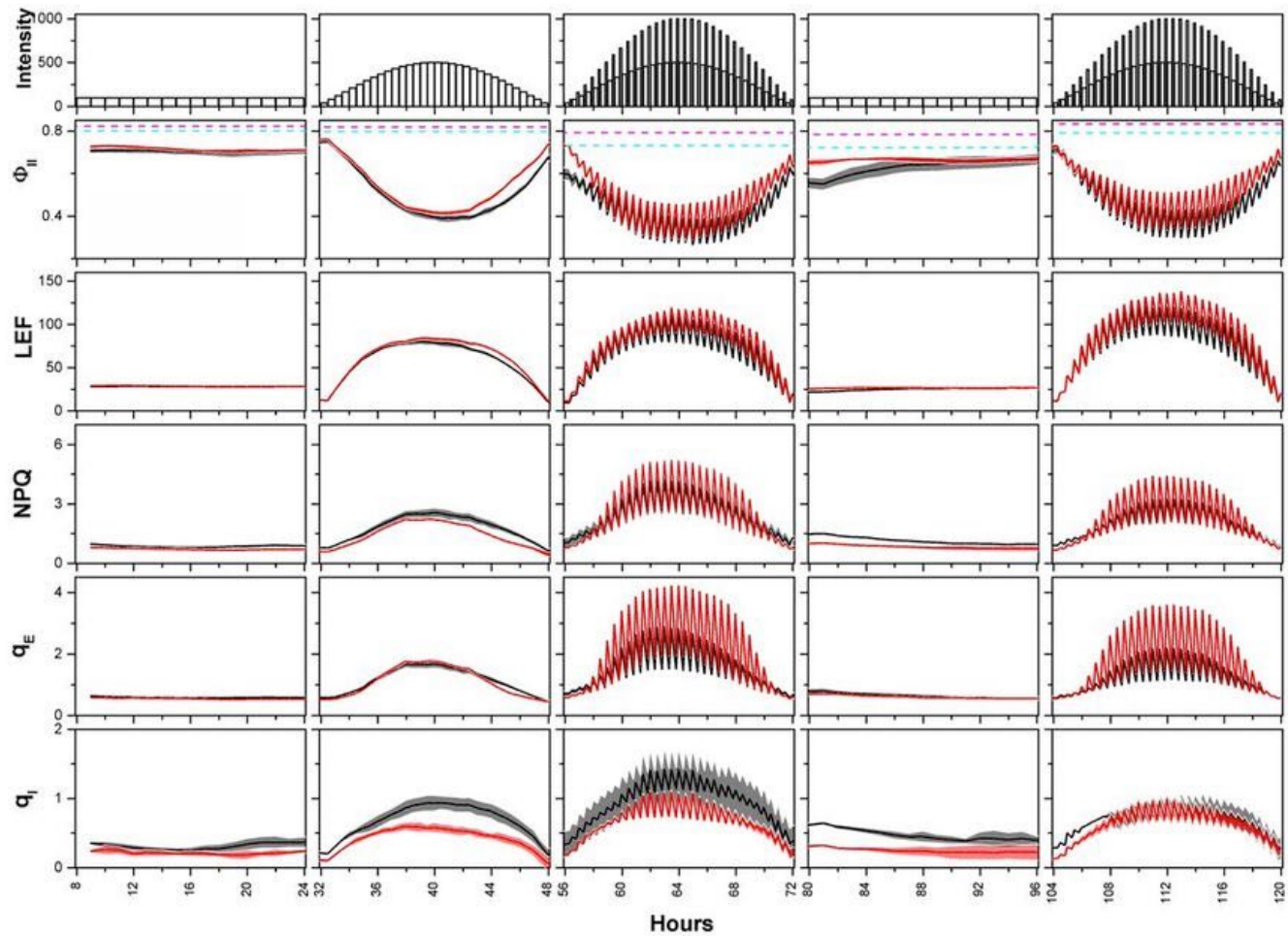


Figure 4

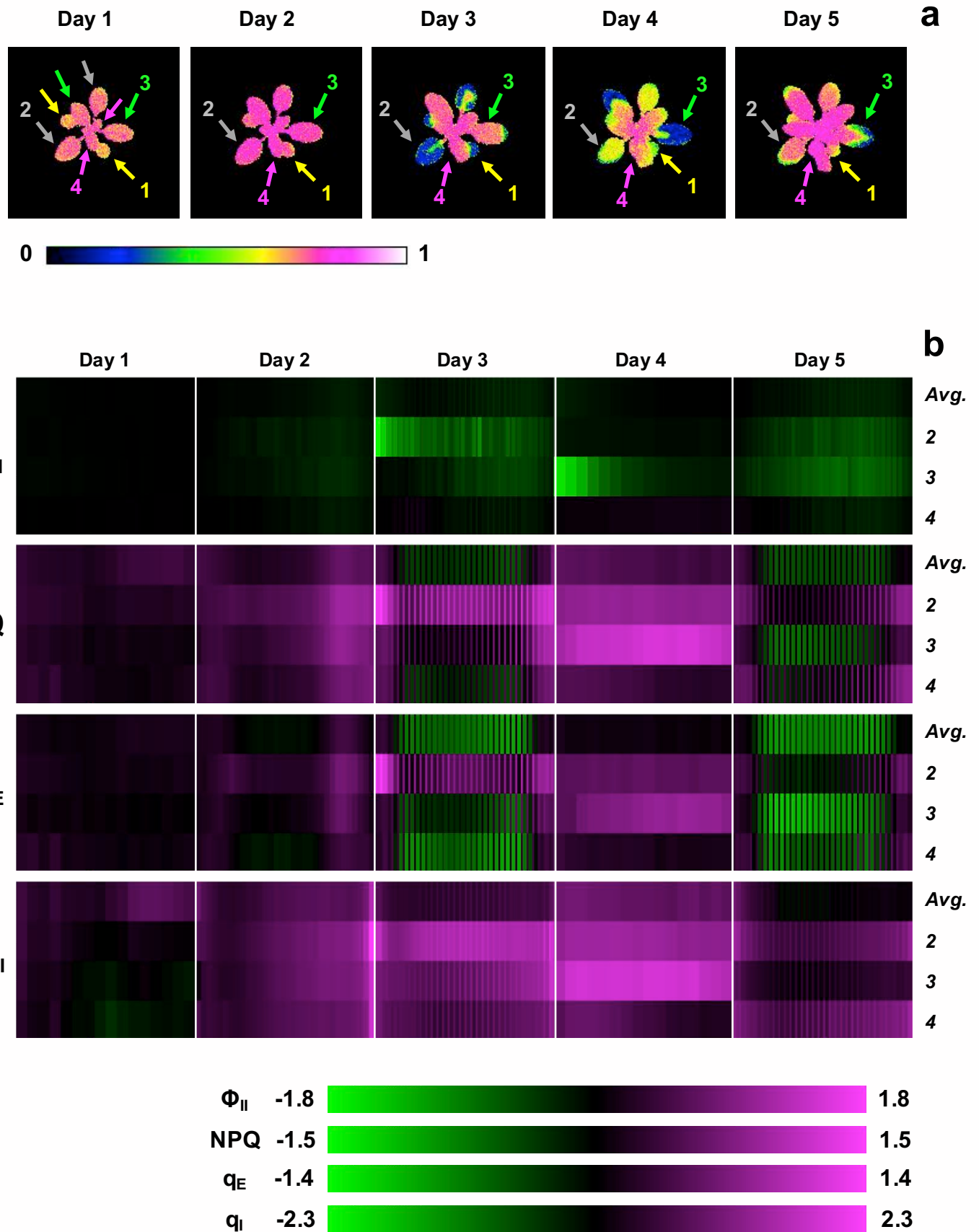


Figure 5

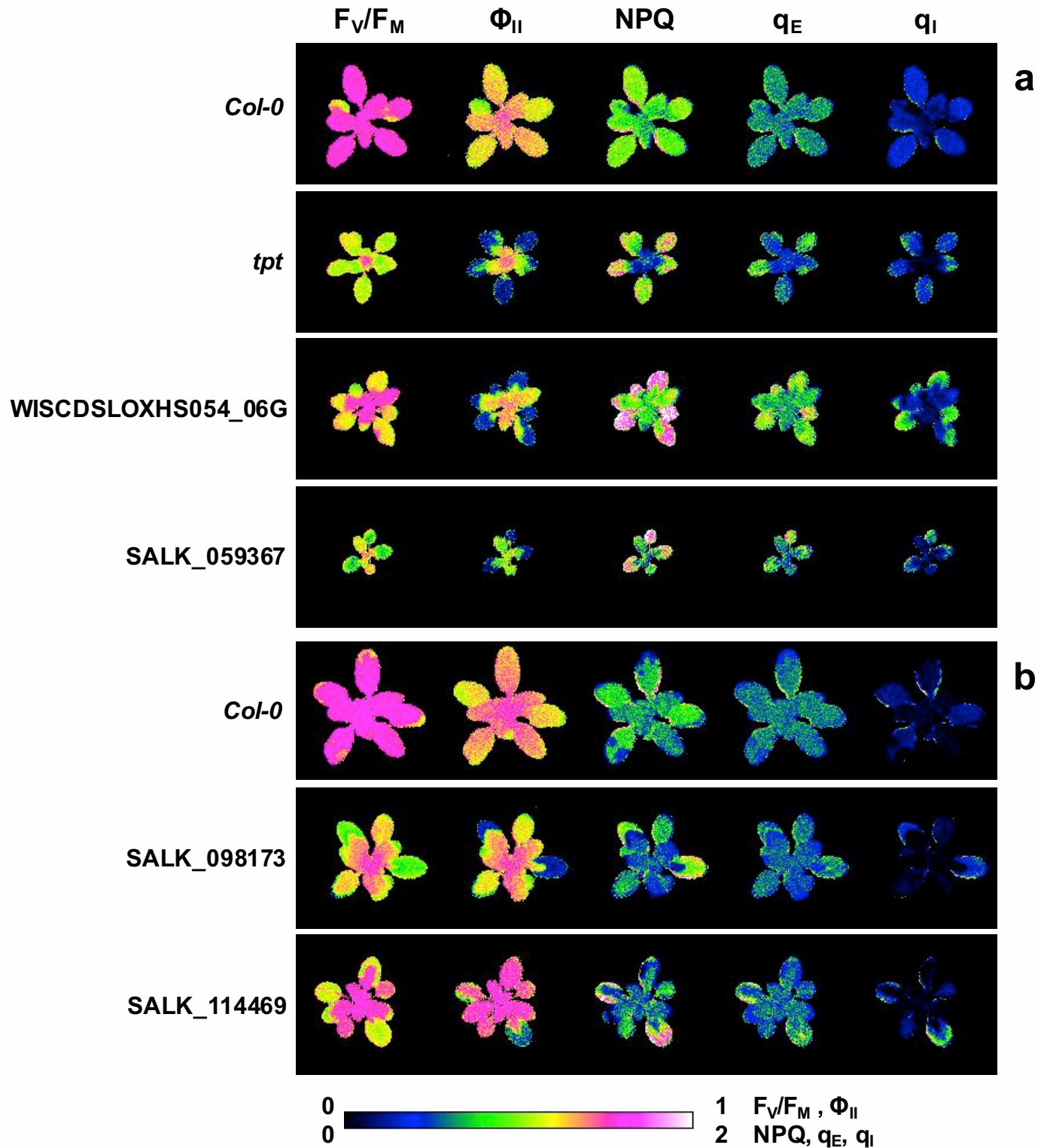
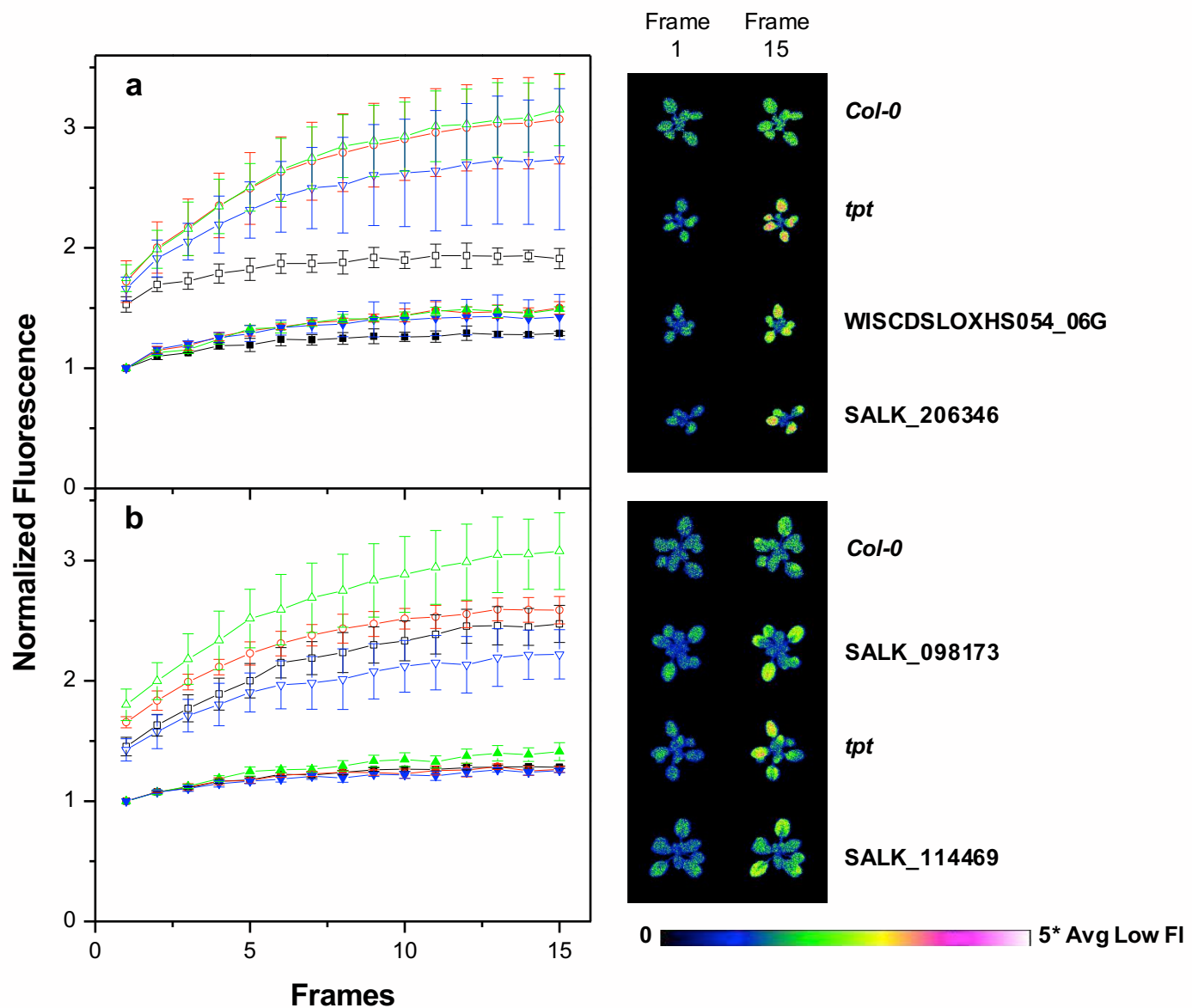
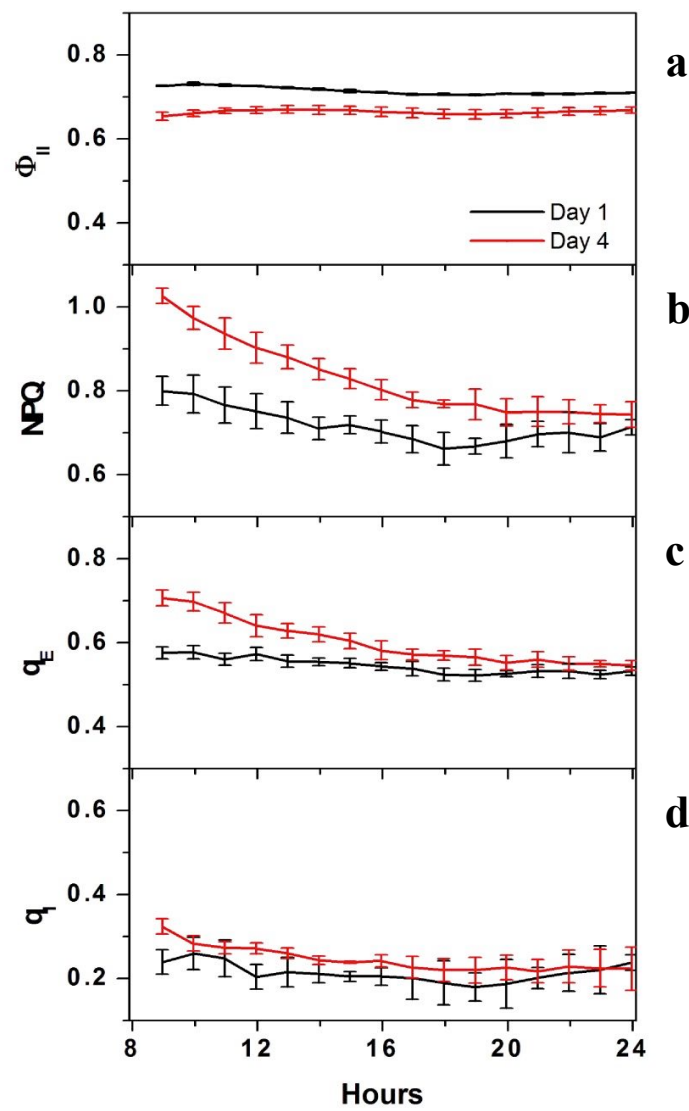
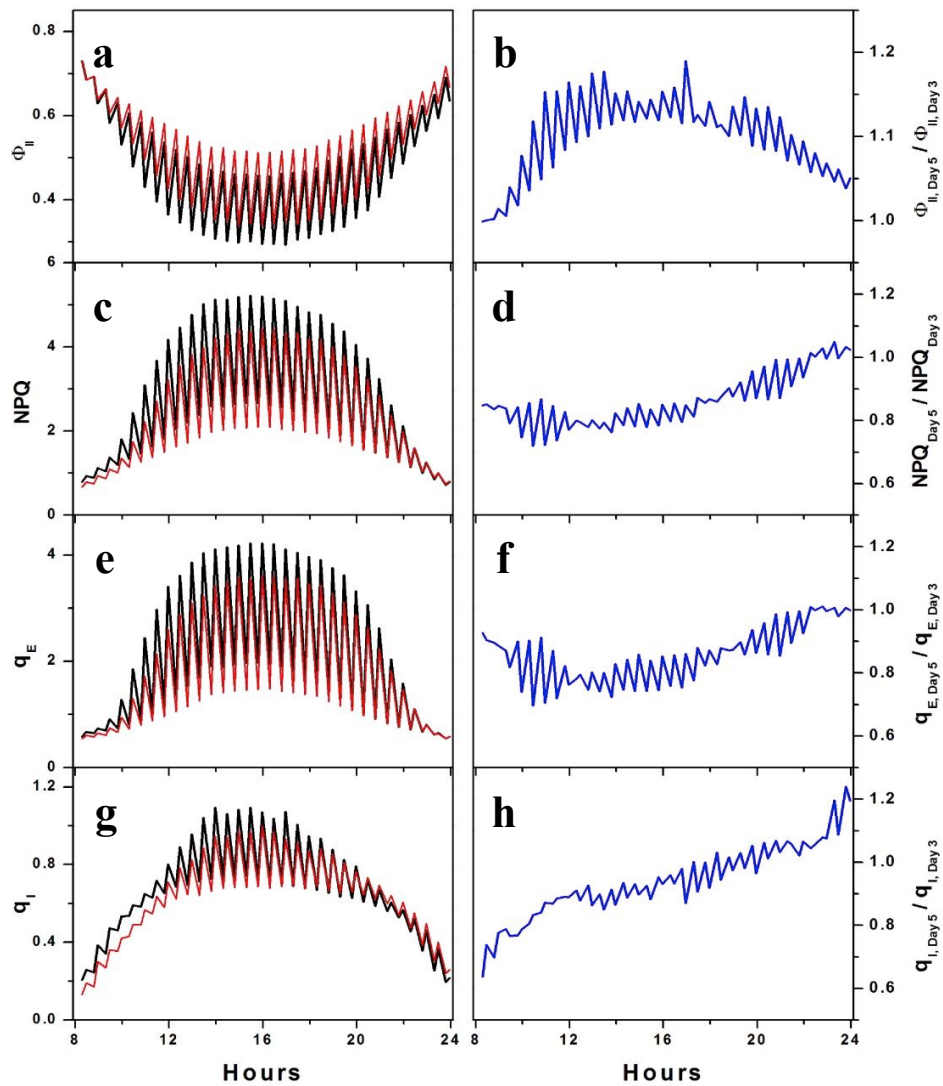


Figure 6

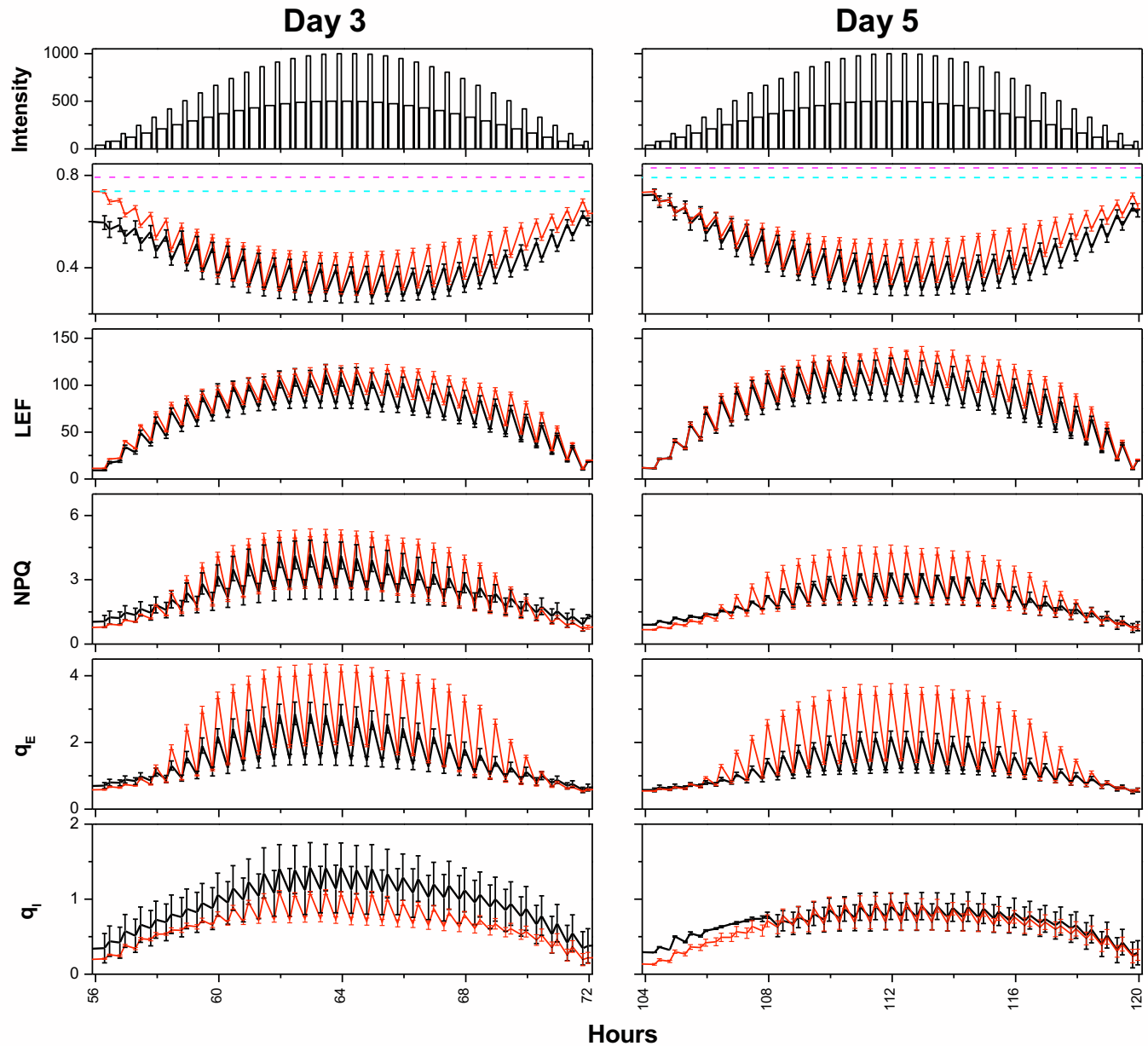




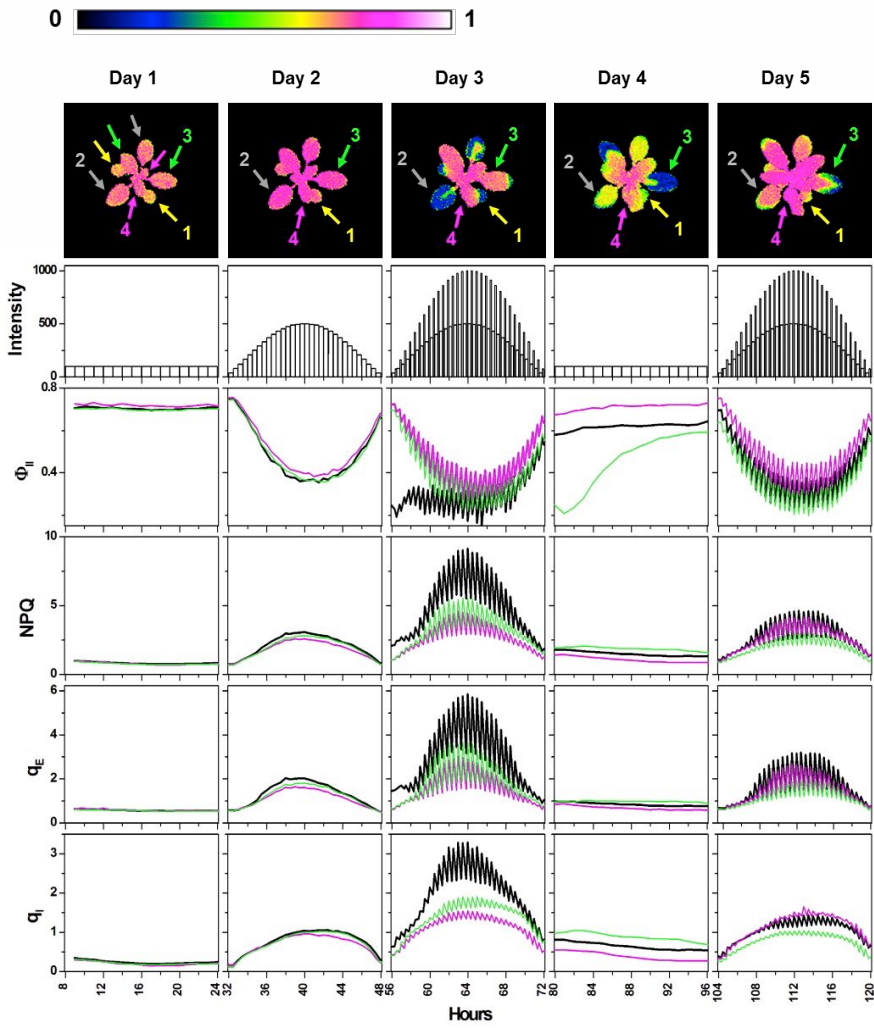
Supplemental Figure 1.
Comparison of photosynthetic performance of Col-0 on days 1 and 4 (Flat days). Averaged surface values of Φ_{II} (a), NPQ (b), q_E (c) and q_I (d), for wild type plants (Col-0) collected on days under which plants were illuminated at a constant intensity of $100 \mu\text{mol photons m}^{-2} \text{s}^{-1}$ (day 1, black and day 4, red).



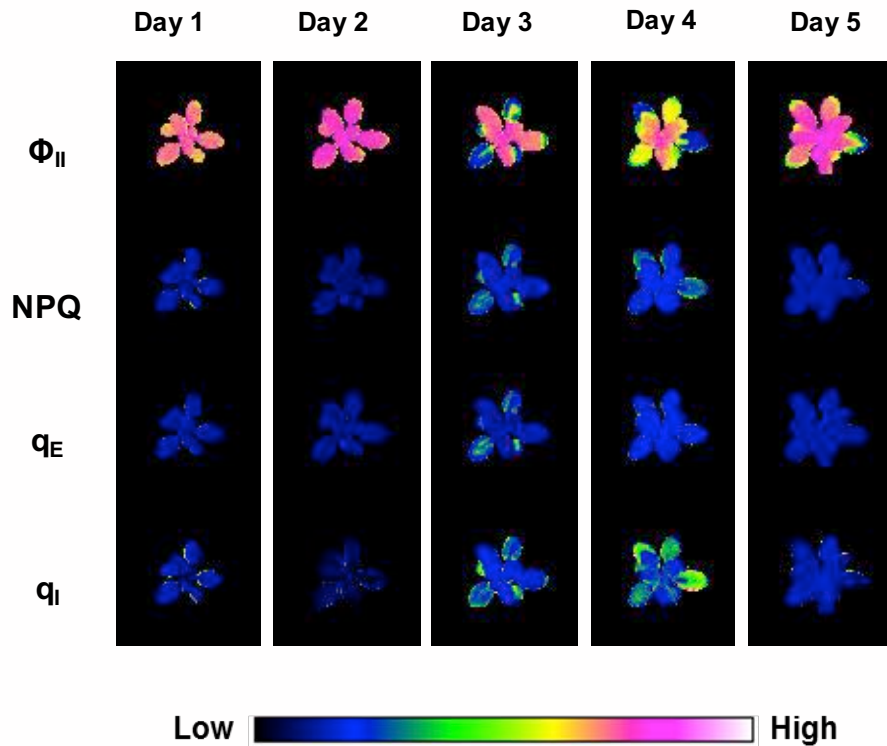
Supplemental Figure 2. Comparison of photosynthetic performance of Col-0 on days 3 and 5 (Flat days). On day 3 and day 5 plants were subjected to fluctuating illumination as shown in Figure 2. Averaged surface values for Col-0 on day 3 (black lines) and day 5 (red lines) and the relative change between the two days (blue lines) in photosynthetic parameters, Φ_{II} (**a** and **b**), NPQ (**c** and **d**), q_E (**e** and **f**) and q_I (**g** and **h**) are plotted against time. Relative change is calculated by dividing values obtained on day 5 by values from corresponding time points on Day 3.



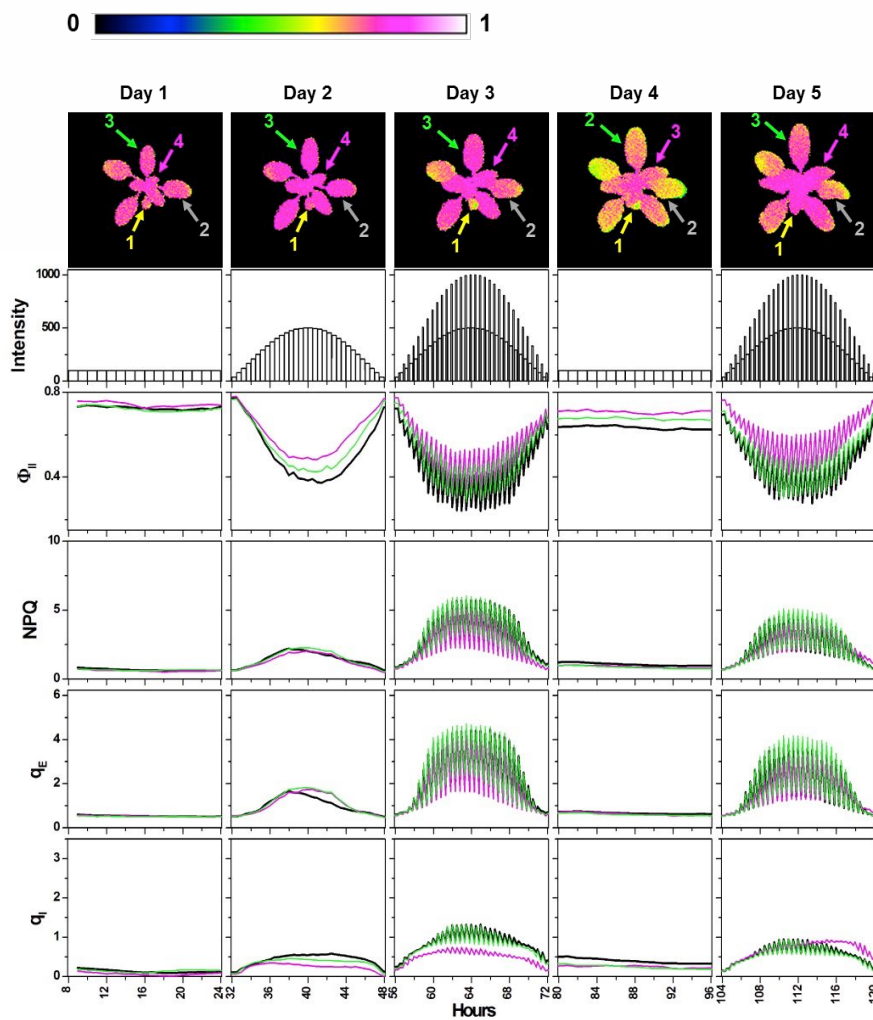
Supplemental Figure 3. Expanded views of emergent phenotypes in SALK_098173 on days 3 and 5 of ramped environmental perturbations. Daily light intensity changes occurring over a days 3 and 5 of ramped environmental perturbations are shown with corresponding averaged ($n=4$) photosynthetic parameters (Φ_{II} , LEF, NPQ, q_E and q_I) for wild type (Col-0, red) and SALK_098173 (SALK_098173, black), with standard deviations represented by the shaded areas. Dashed magenta (Col-0) and cyan (SALK_098173) lines in the plots of Φ_{II} indicate averaged F_v/F_m values.



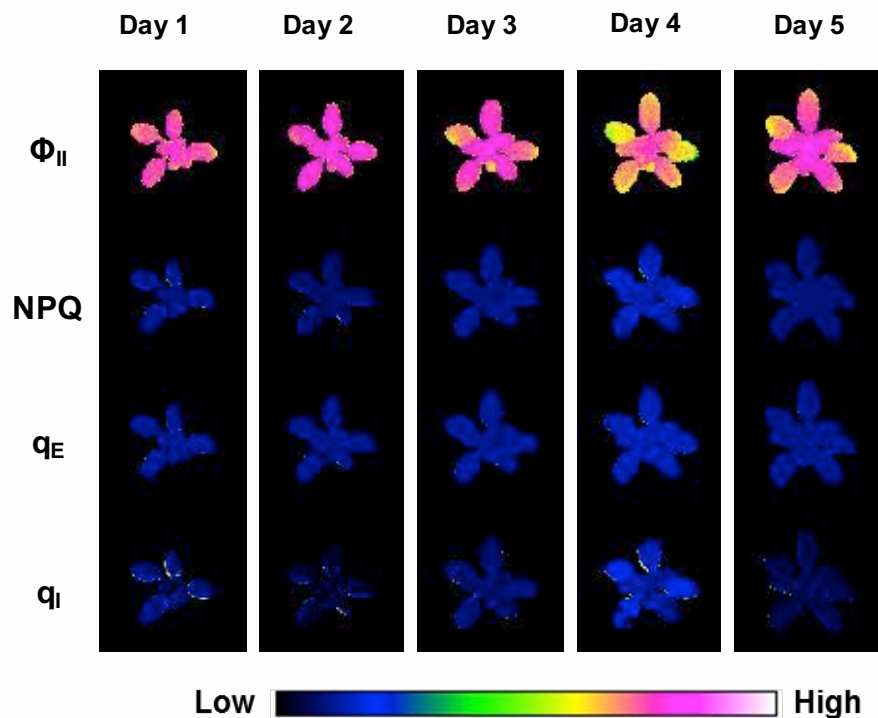
Supplemental Figure 4. Spatial and temporal heterogeneity of photosynthesis in SALK_098173. False color Φ_{II} images of SALK_098173 in the morning of each day of measurement. Arrows point towards a cotyledon (*yellow, leaf 1*) a first rosette leaf (*grey, leaf 2*), a second rosette leaf (*green, leaf 3*) and a third rosette leaf (*magenta, leaf 4*). Over 5 days of varied light intensity changes (uppermost graph) average values of photosynthetic parameters (graphs descending order; Φ_{II} , NPQ, q_E , q_I) were tracked a small area of fixed size on a first rosette leaf (*black lines, leaf 2*), a second rosette leaf (*green lines, leaf 3*) and a third rosette leaf (*magenta lines, leaf 4*).



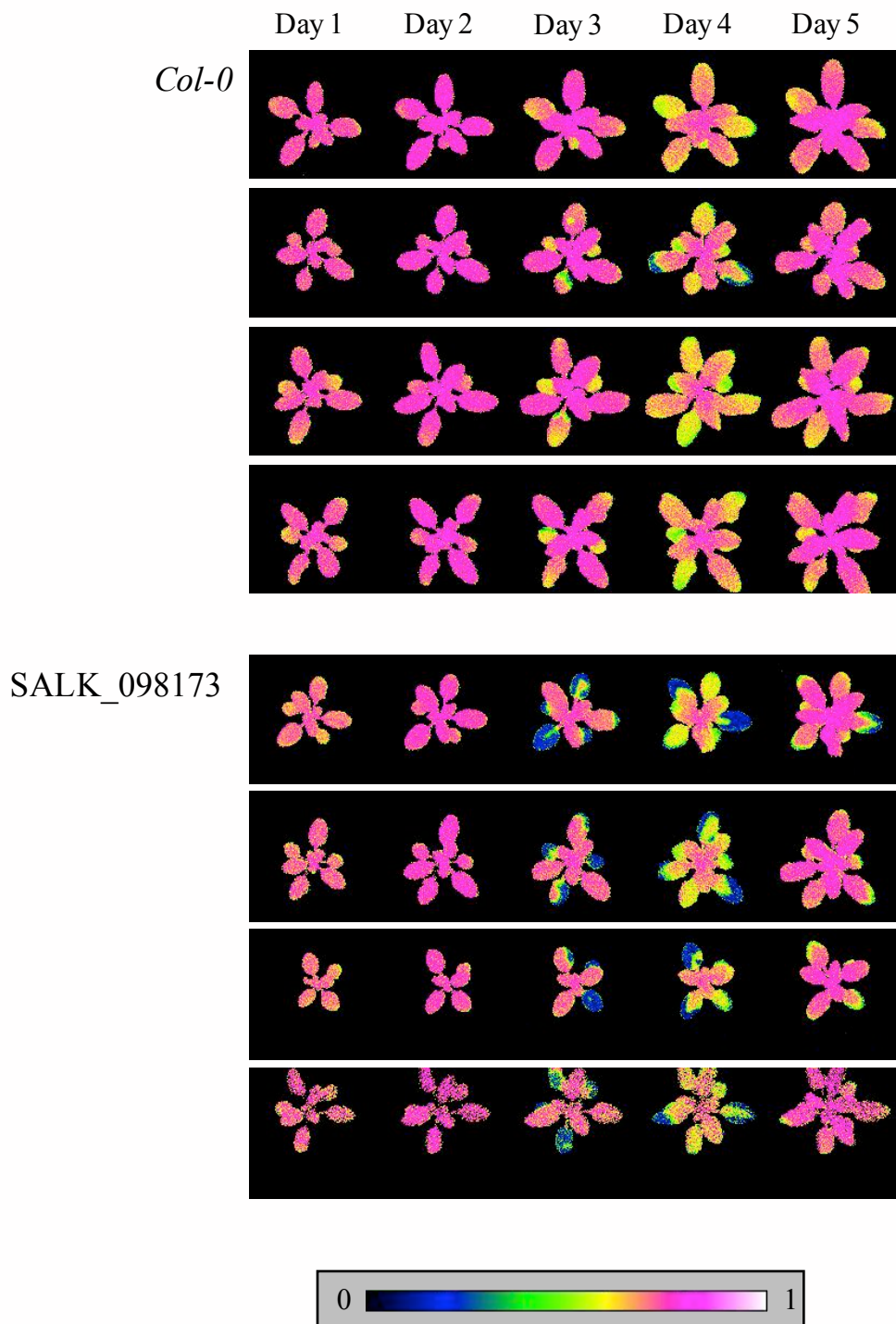
Supplemental Video 1. Spatial and temporal heterogeneity of photosynthesis in SALK_098173. False color videos of Φ_{II} , NPQ, q_E , q_I in SALK_098173 over 5 days of varied light intensity changes as described in **Supplementary Figure 3**.



Supplemental Figure 5. Spatial and temporal heterogeneity of photosynthesis in Col-0. False color Φ_{II} images of a wild type (Col-0) plant in the morning on the each day of measurement. Arrows point towards a cotyledon (yellow, leaf 1) a first rosette leaf (grey, leaf 2), a second rosette leaf (green, leaf 3) and a third rosette leaf (magenta, leaf 4). Over 5 days of varied light intensity changes (uppermost graph) average values of photosynthetic parameters (graphs descending order; Φ_{II} , NPQ, q_E , q_I) were tracked a small area of fixed size on a first rosette leaf (black lines, leaf 2), a second rosette leaf (green lines, leaf 3) and a third rosette leaf (magenta lines, leaf 4).



Supplemental Video 2. Spatial and temporal heterogeneity of photosynthesis in Col-0. False color videos of Φ_{II} , NPQ, q_E , q_I in a wild type (Col-0) over 5 days of varied light intensity changes as described in **Supplemental Figure 4**.

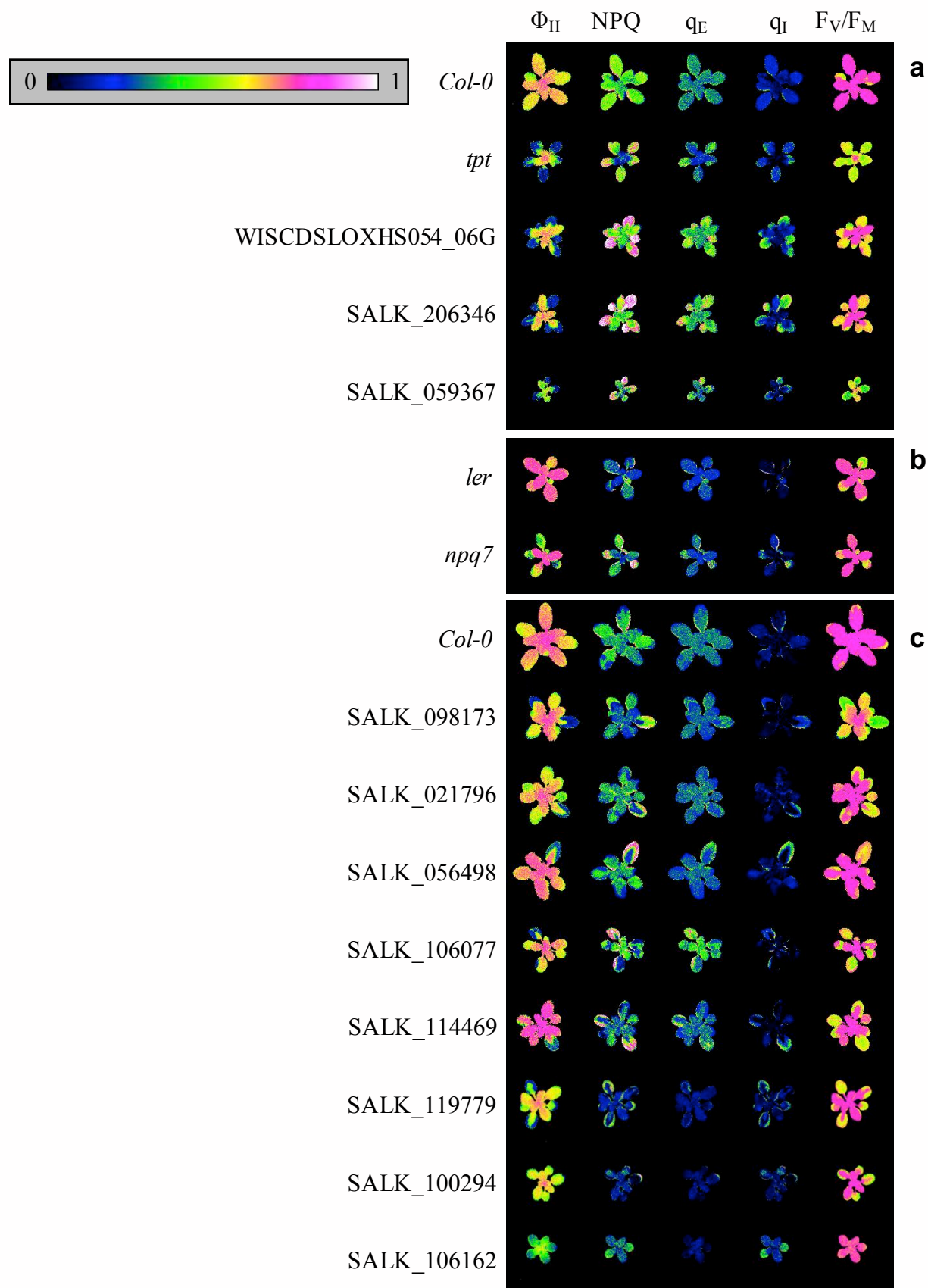


Supplemental Figure 6. Replicates of SALK_098173. False color images of Φ_{II} for 4 replicates of SALK_098173 and the corresponding *Col-0* controls over the 5 day experiment.

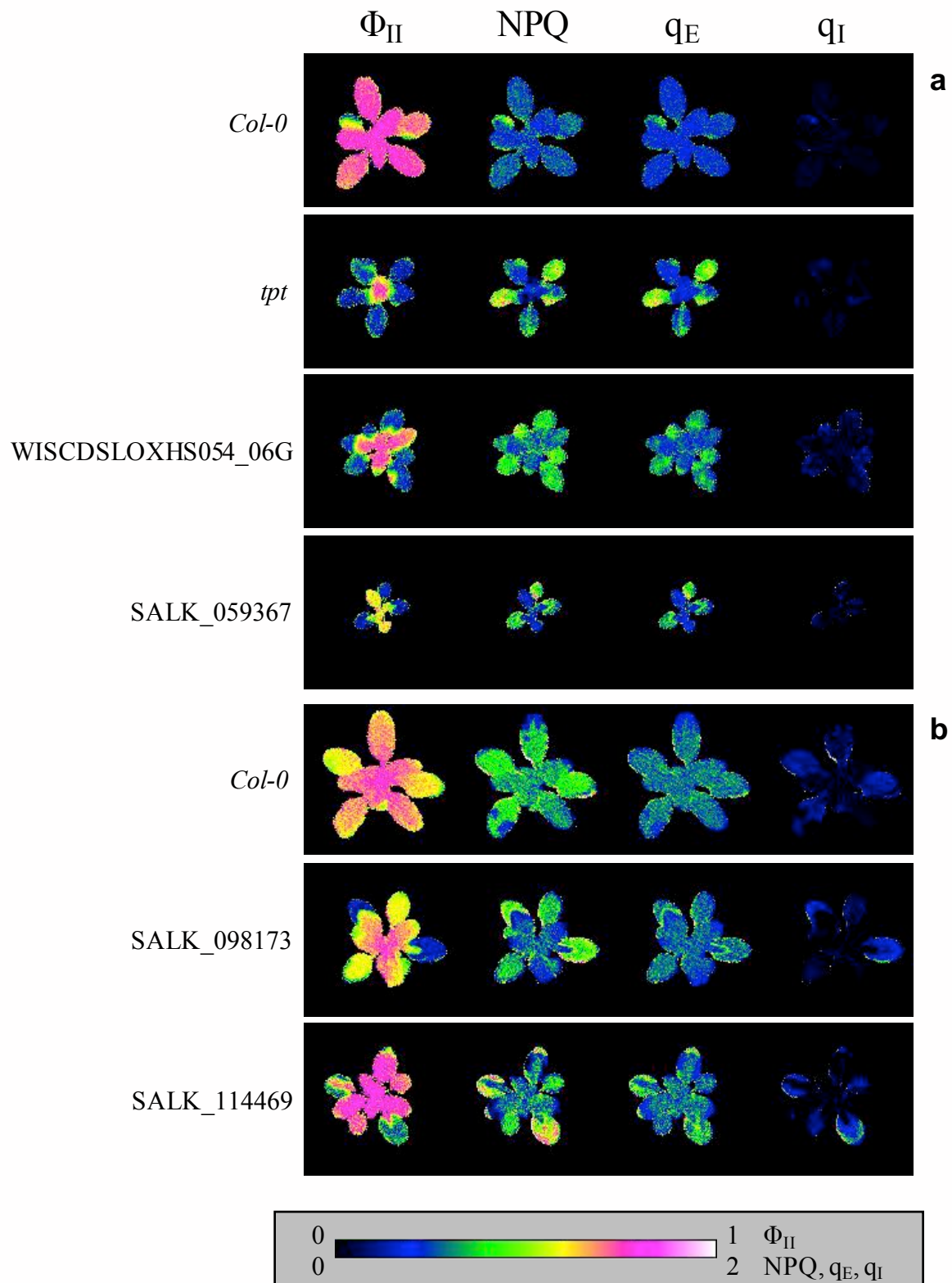
Supplemental Table 1. Arabidopsis mutant lines exhibiting patchy phenotypes. In addition to the published lines, second alleles for WISCD SLOXHS054_06G similar results, and a complemented line for SALK_098173 suppresses the phenotype, suggesting that the disruption of the indicated genes are were likely responsible for the patchy phenotypes.

Line	Additional allele(s)	Locus	Abbreviated Annotation	Patchiness observed	References
<i>npq7</i>		At1g65420	Chloroplast localized YCF20-like gene involved in nonphotochemical quenching	End of days 2 and 3	Jung et al., 2010
<i>tpt</i>		At5g46110	Chloroplast triose phosphate / 3-phosphoglycerate translocator	Beginning of days 1, 2, 3 and 4	Schneider et al., 2002
WISCD SLOXHS054_06G	SALK_206346	At1g16880	Encodes a ACT domain-containing protein	Beginning of days 2, 3 and 4*	
SALK_059367		At3g46610	Pentatricopeptide repeat (PPR-like) superfamily protein	Beginning of days 3 and 4	
SALK_098173		At1g71500	PSB33 is associated with the chloroplast thylakoid membrane and provides stability to Photosystem II	Beginning of days 3 and 4	Fristedt et al., 2002
SALK_021796	SAIL_335_F05	At5g59250	Major facilitator superfamily protein	Beginning of day 4	
SALK_056498	SALK_095654 SALK_202821	At1g18730	NDF6, Photosynthetic NDH subcomplex B 4	Beginning of day 4	Ishikawa et al., 2008
SALK_106077		At3g10470	C2H2-type zinc finger family protein	Beginning of day 4	Shin et al., 2015 Kim S-G et al., 2010
SALK_114469		At1g79040	PSBR; subunit of photosystem II (PSII); This subunit appears to be involved in the stable assembly of PSII	Beginning of day 4	Liu et al., 2009 Allahverdiyeva et al., 2013
SALK_119779	SALK_010971	At5g01500	TAAC; ATP/ADP carrier localized to the thylakoid membrane	Beginning of day 4	Thuswaldner et al. 2007
SALK_100294	SAIL_588_H04	At5g08540	unknown protein	Beginning of day 4	
SALK_106162	SALK_034514	At2g29180	unknown protein	Beginning of day 2, 3, 4	

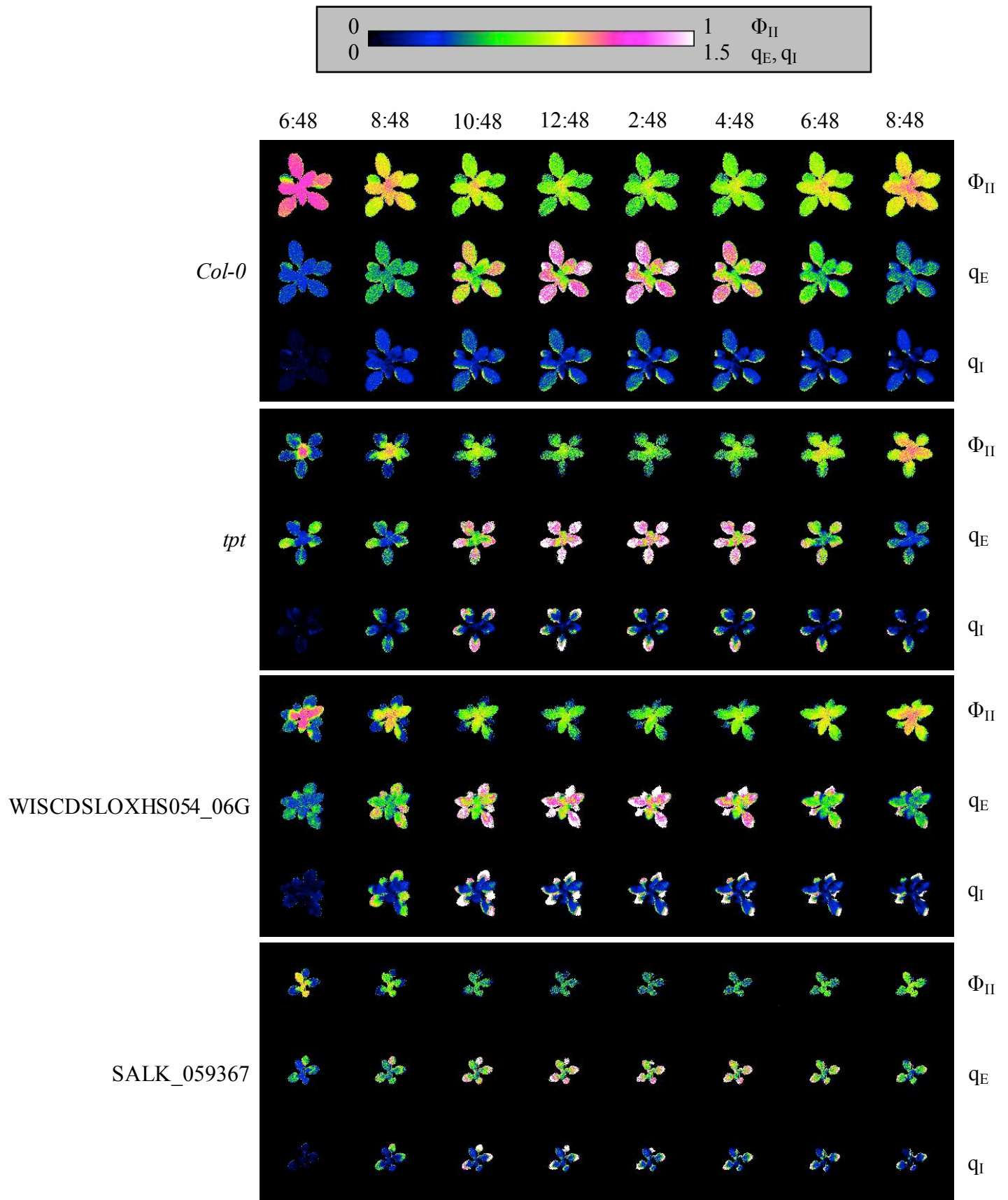
*Leaf senescence observed on day 4.



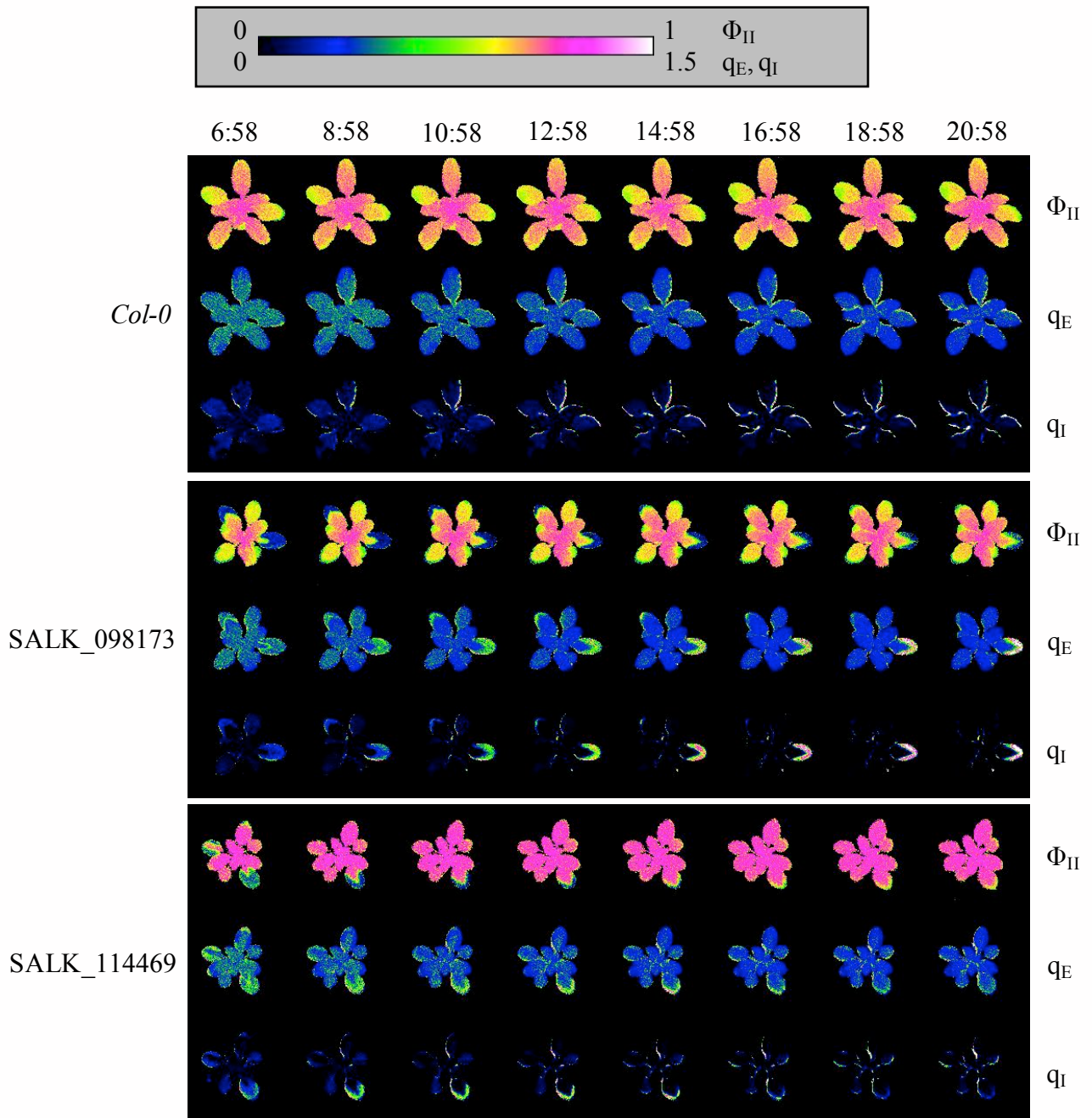
Supplemental Figure 7. Photosynthetic snapshots of “patchy” phenotype mutants. Representative false color images of F_V/F_M and of Φ_{II} , NPQ, q_E and q_I after (a) ~2 hours of actinic illumination on day 3, (b) ~15.5 hours of illumination on day 3 and (c) ~1 hour of illumination on day 4, for patchy mutant lines listed in Supplemental Table 1. SALK_206346 in panel a is a second allele of WISCDSLOXHS054_06G.



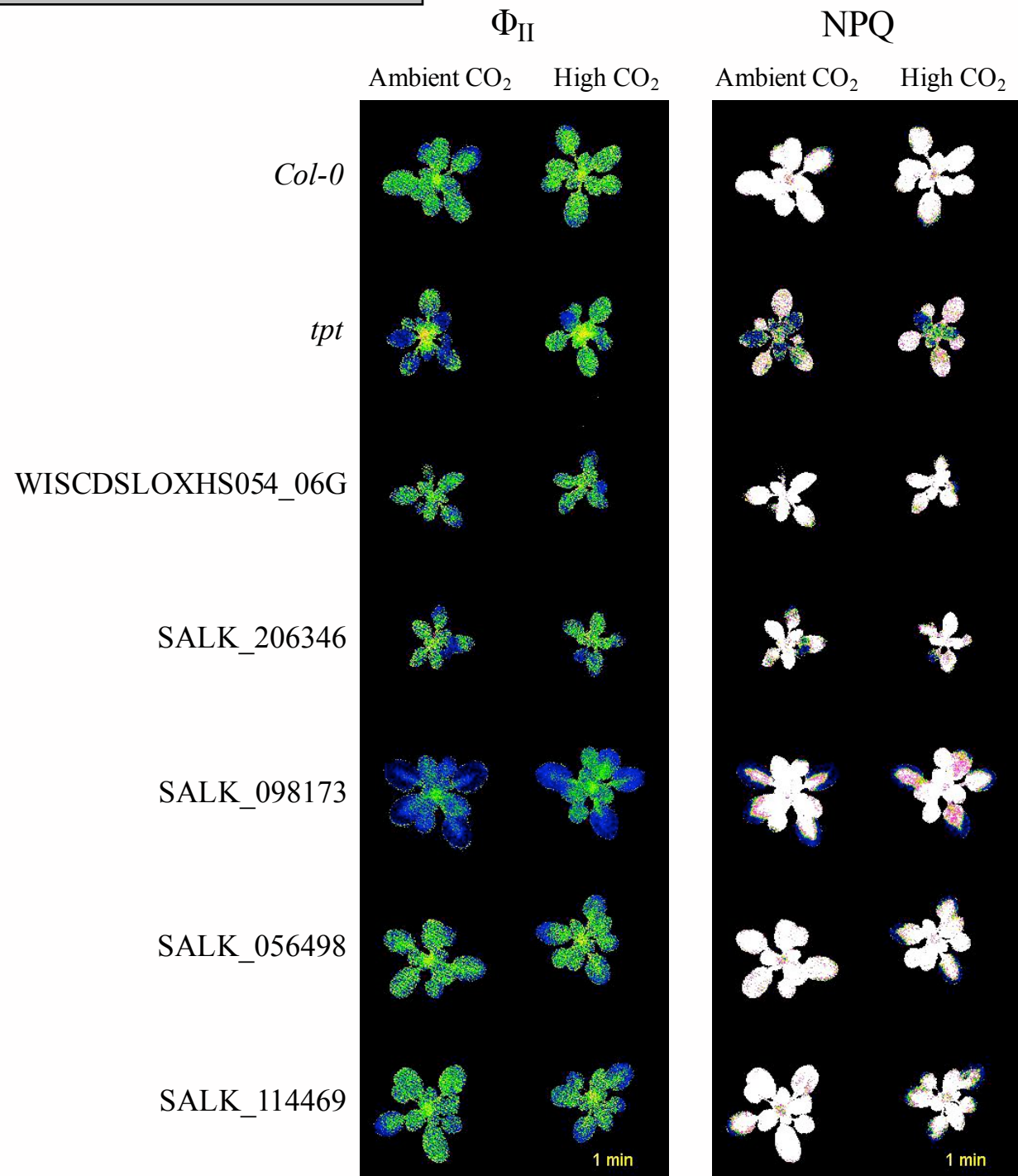
Supplemental Video 3. Progressive changes in the photosynthetic performance of patchy mutants. Movies show false color images of Φ_{II} , NPQ, q_E and q_I over the course of a) day 3; *Col-0*, *tpt*, WISCD SLOXHS054_06G and SALK_059367 and b) day 4; *Col-0*, SALK_098173 and SALK_114469).



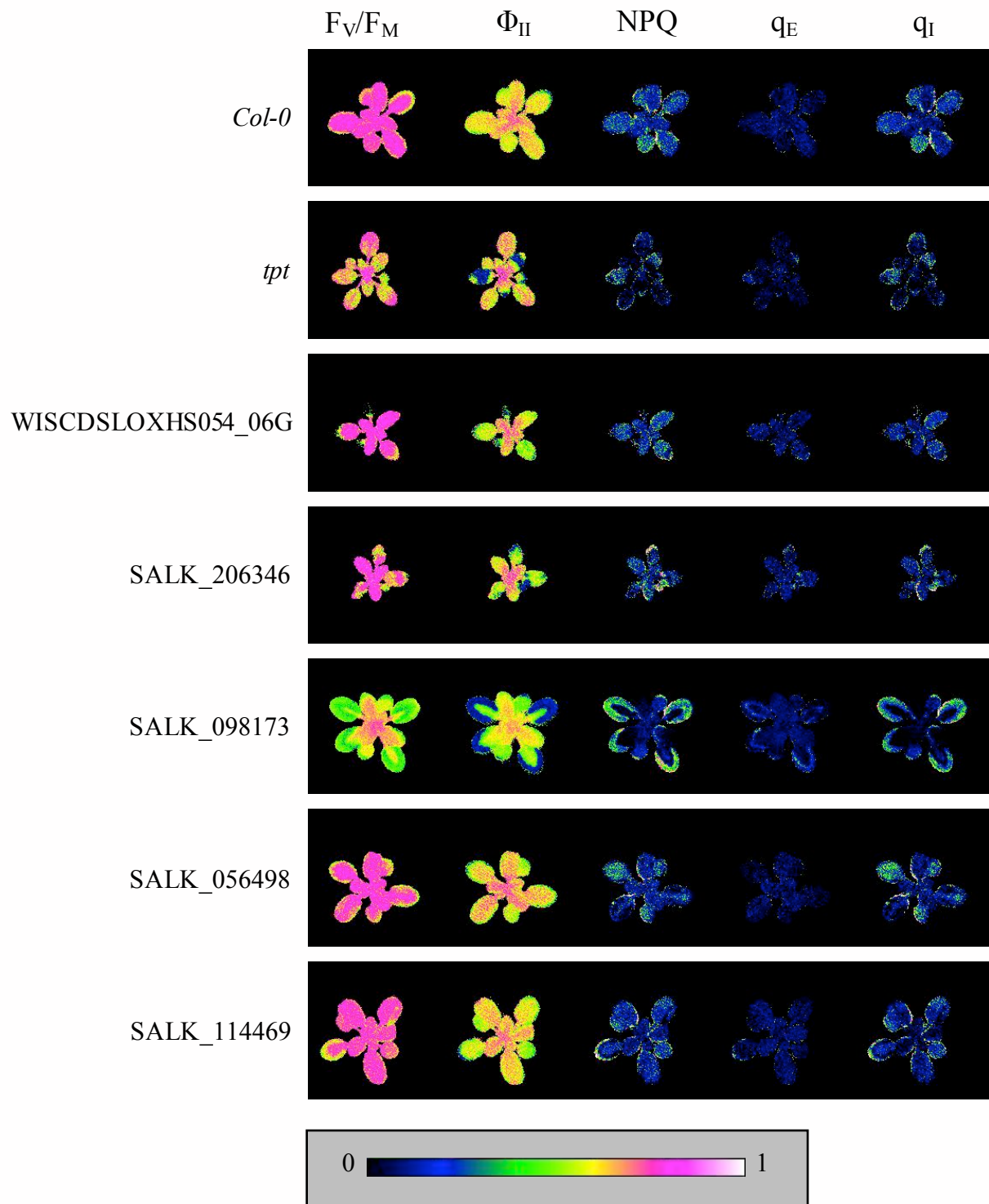
Supplementary Figure 8. Progressive and localized changes in quantum yield and quenching. Time course of Φ_{II} and q_E and q_I , over day 3 for *Col-0*, *tpt*, WISCD SLOXHS054_06G, SALK_059367.



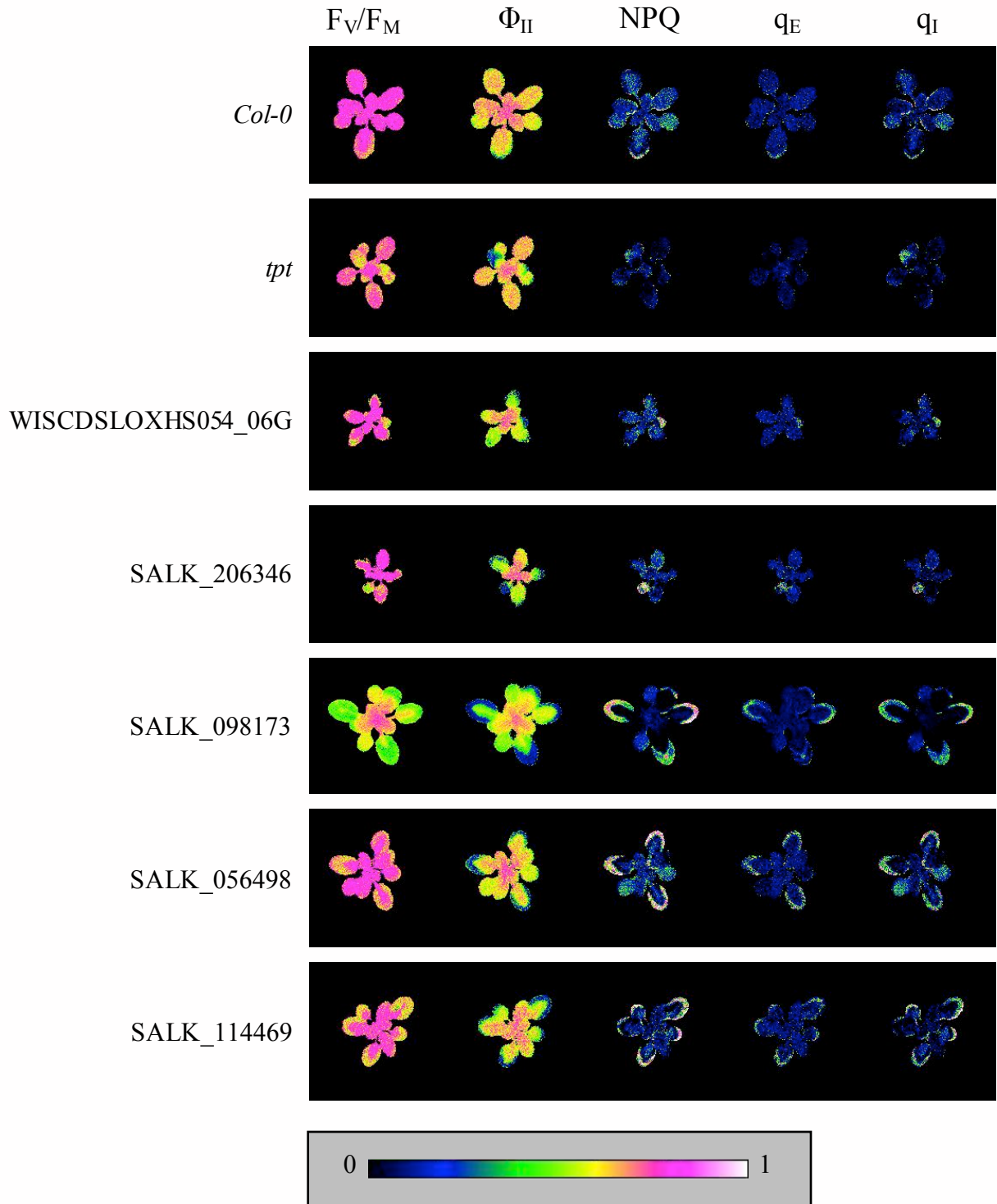
Supplemental Figure 9. Progressive and localized changes in quantum yield and quenching. Time course of Φ_{II} , q_E and q_I , over day 4 for Col-0, SALK_098173 and SALK_114469. The photoperiod started at 6:00 AM and ended at 10:00 PM (22:00).



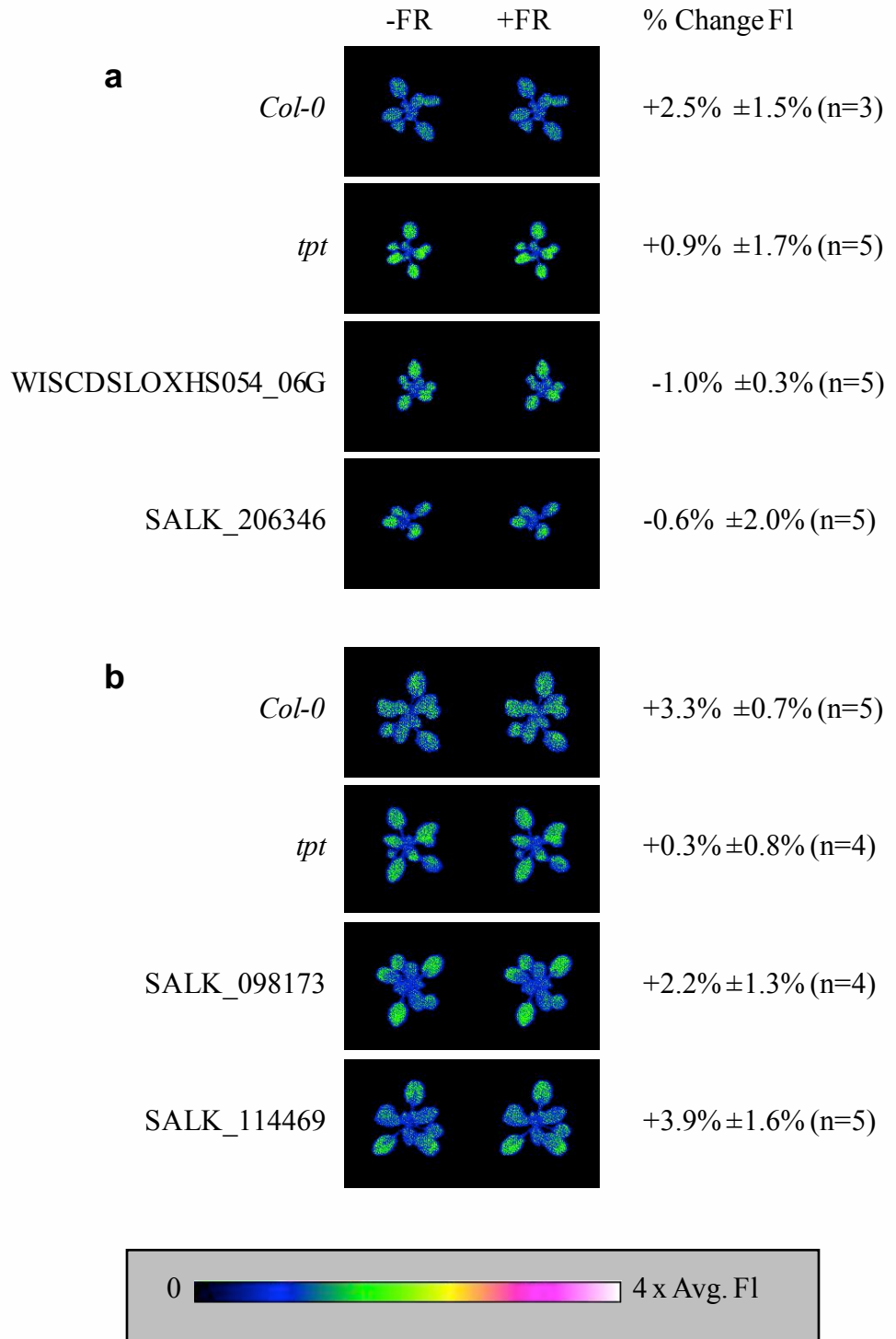
Supplemental Video 4. Effect of high CO₂ on the patchy phenotype for a select subset of mutants. One hour prior to the start of day 4, CO₂ concentration was increased to ~2500 ppm inside the DEPI chamber for a period of 2 hours. Movies show false color images of Φ_{II} (*left*) and NPQ (*right*) for representative plants (*Col-0*, *tpt*, WISCD SLOXHS054_06G, SALK_206346, SALK_098173, SALK_056498 and SALK_114469) collected during the first 2 hours of illumination under ambient and high CO₂.



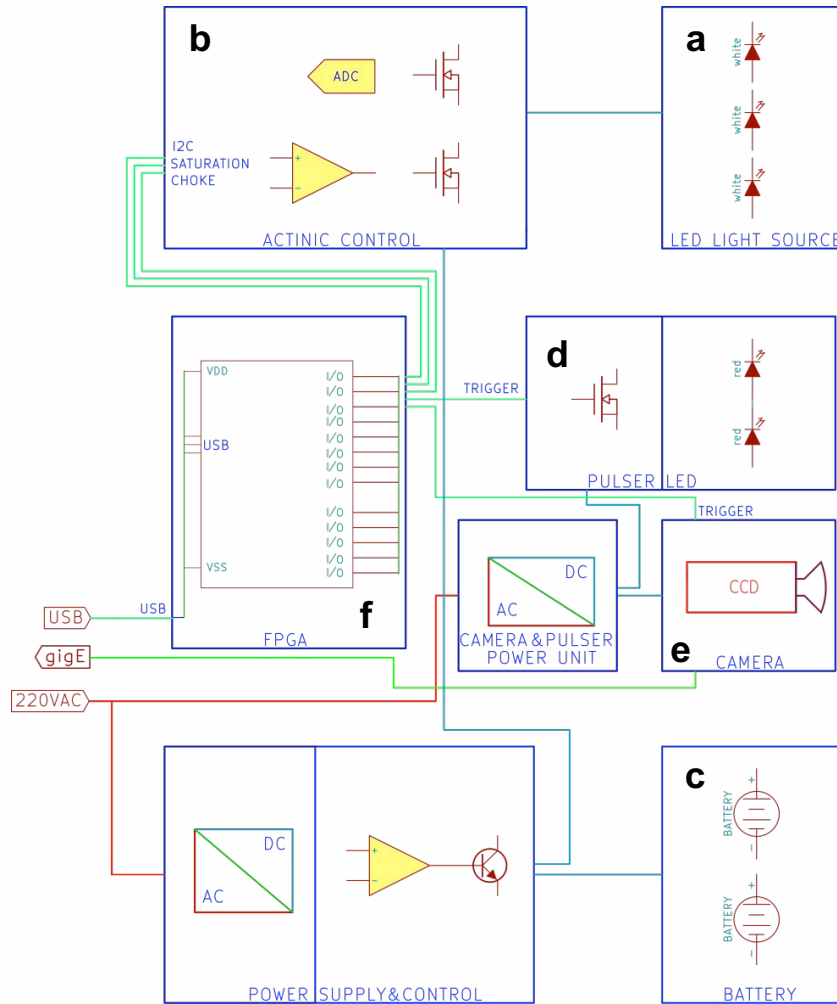
Supplemental Figure 10. Photosynthetic parameters under ambient CO₂. Representative false color images of F_v/F_m and of Φ_{II} , NPQ, q_E and q_I after ~1 hour of actinic illumination for mutant lines (*tpt*, WISCD SLOXHS054_06G, SALK_206346, SALK_098173, SALK_056498, SALK_114469) background line (*Col-0*): A) at the beginning of Day 4 under ambient CO₂.



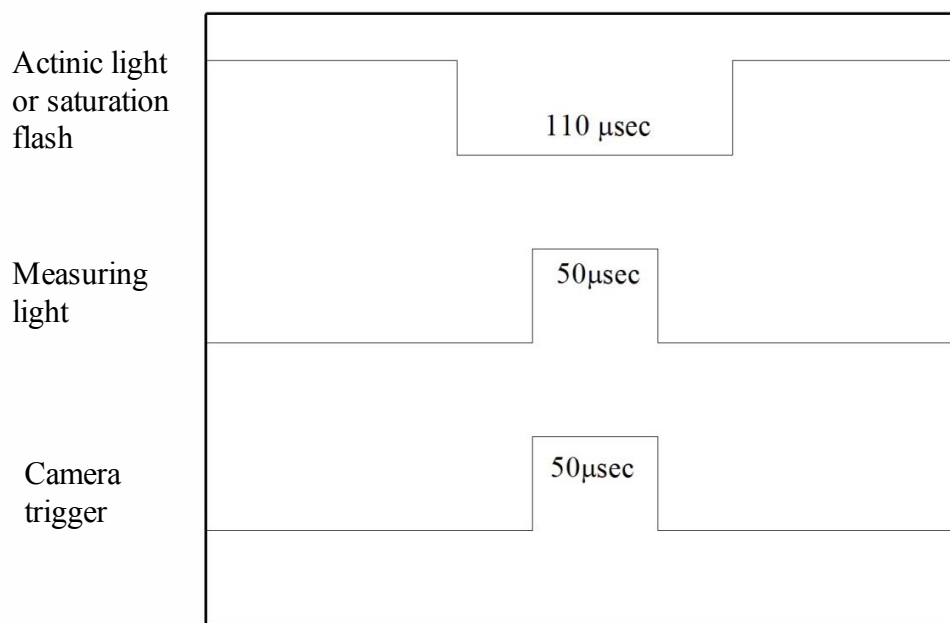
Supplemental Figure 11. Photosynthetic parameters under elevated CO₂. Representative false color images of F_v/F_m and of Φ_{II} , NPQ, q_E and q_I after ~1 hour of actinic illumination for mutant lines (*tpt*, WISCD SLOXHS054_06G, SALK_206346, SALK_098173, SALK_056498, SALK_114469) background line (*Col-0*): A) at the beginning of day 4 under 2 hours of 2,500 ppm CO₂, as explained in the legend for Supplemental video 3.



Supplemental Figure 12. Far red treatment does not rescue the high F₀ phenotype.
 Chlorophyll fluorescence images were collected on dark adapted (pre-dawn) mutant (*tpt*, WISCD SLOXHS054_06G and SALK_206346 on day 3 for group *a*; *tpt*, SALK_098173 and SALK_114469 on day 4 for group *b*) and *Col-0* plants, before (-FR) and after illumination with far-red LEDs (peak wavelength 720 nm) for 25 seconds. Shown above in false color are averaged fluorescence images from the first 2 frames (of a 15 frame measurement). Shown also is the percent change in the average fluorescence intensity after treatment with far-red illumination.



Supplemental Figure 13. Technical Schematic for DEPI. Output intensity of an array of white 50W LEDs (**a**) was regulated by a master computer via I²C bus to set ADC output, controlling the LED current by a voltage to current control circuit (**b**). Saturation pulse illumination was achieved by pulsing the LED array at high current using supplementary lead acid battery power (**c**). Monochromatic (red) probe LEDs were controlled through a rapid gating circuit using MOSFETS (**d**). Signals for setting light intensity, gating actinic light, gating the saturation pulse (**b**), controlling measuring pulses (**d**) and triggering high resolution CCD Gigabit Ethernet (GigE) cameras (**e**) were generated by a 50 MHz resolution digital programmable timer by programming a field-programmable gate array or FPGA (**f**).



Supplemental Figure 14. Timing diagram for capture of a single fluorescence image during actinic or saturating illumination.

Image capture by CCD camera over a 50 μsec window is synchronized with a 50 μsec pulse of probe light, occurring during a ~100 μsec window when actinic or saturating illumination is turned off.